Projecting genetic associations through gene expression patterns highlights disease etiology and drug mechanisms

This manuscript ([permalink](#)) was automatically generated from [greenelab/phenoplier_manuscript@1833e89](#) on July 1, 2021.

Authors

- **Milton Pividori**
  [0000-0002-3035-4403](#) · ⦿ [miltondp](#) · 🐦 [miltondp](#)
  Department of Genetics, Perelman School of Medicine, University of Pennsylvania, Philadelphia, PA 19104, USA · Funded by The Gordon and Betty Moore Foundation GBMF 4552; The National Human Genome Research Institute (R01 HG010067)

- **Sumei Lu**

  Center for Spatial and Functional Genomics, Children's Hospital of Philadelphia, Philadelphia, PA, 19104, USA

- **Binglan Li**
  [0000-0002-0103-6107](#)
  Department of Biomedical Data Science, Stanford University, Stanford, CA, USA

- **Chun Su**
  [0000-0001-6388-8666](#) · ⦿ [sckinta](#)
  Center for Spatial and Functional Genomics, Children's Hospital of Philadelphia, Philadelphia, PA, 19104, USA

- **Matthew E. Johnson**

  Center for Spatial and Functional Genomics, Children's Hospital of Philadelphia, Philadelphia, PA, 19104, USA

- **Wei-Qi Wei**

  Vanderbilt University Medical Center

- **Qiping Feng**
  [0000-0002-6213-793X](#)
  Vanderbilt University Medical Center

- **Bahram Namjou**

  Cincinnati Children's Hospital Medical Center

- **Krzysztof Kiryluk**
  [0000-0002-5047-6715](#) · 🐦 [kirylukk](#)
  Department of Medicine, Division of Nephrology, Vagelos College of Physicians & Surgeons, Columbia University, New York, New York

- **Iftikhar Kullo**

  Mayo Clinic

- **Yuan Luo**

  Northwestern University

- **Blair D. Sullivan**

  School of Computing, University of Utah, Salt Lake City, UT, USA

- **Carsten Skarke**
  ⓘD 0000-0001-5145-3681 · 🐦 CarstenSkarke
  Institute for Translational Medicine and Therapeutics, Department of Medicine, University of Pennsylvania, Philadelphia, PA 19104, USA

- **Marylyn D. Ritchie**
  ⓘD 0000-0002-1208-1720 · 🐦 MarylynRitchie
  Department of Genetics, Perelman School of Medicine, University of Pennsylvania, Philadelphia, PA 19104, USA

- **Struan F.A. Grant**
  ⓘD 0000-0003-2025-5302 · 🐦 STRUANGRANT
  Center for Spatial and Functional Genomics, Children's Hospital of Philadelphia, Philadelphia, PA, 19104, USA; Department of Pediatrics, Perelman School of Medicine, University of Pennsylvania, Philadelphia, PA, 19104, USA; Division of Human Genetics, Children's Hospital of Philadelphia, Philadelphia, PA, 19104, USA

- **Casey S. Greene**
  ⓘD 0000-0001-8713-9213 · ⓖ cgreene · 🐦 GreeneScientist
  Center for Health AI, University of Colorado School of Medicine, Aurora, CO 80045, USA; Department of Biochemistry and Molecular Genetics, University of Colorado School of Medicine, Aurora, CO 80045, USA · Funded by The Gordon and Betty Moore Foundation (GBMF 4552); The National Human Genome Research Institute (R01 HG010067); The National Cancer Institute (R01 CA237170)

Abstract

Understanding how dysregulated transcriptional processes result in tissue-specific pathology requires a mechanistic interpretation of expression regulation across different cell types. It has been shown that this insight is key for the development of new therapies. These mechanisms can be identified with transcriptome-wide association studies (TWAS), which have represented an important step forward to test the mediating role of gene expression in GWAS associations. However, due to pervasive eQTL sharing across tissues, TWAS has not been successful in identifying causal tissues, and other methods generally do not take advantage of the large amounts of RNA-seq data publicly available. Here we introduce a polygenic approach that leverages gene modules (genes with similar co-expression patterns) to project both gene-trait associations and pharmacological perturbation data into a common latent representation for a joint analysis. We observed that diseases were significantly associated with gene modules expressed in relevant cell types, such as hypothyroidism with T cells and thyroid, hypertension and lipids with adipose tissue, and coronary artery disease with cardiomyocytes. Our approach was more accurate in predicting known drug-disease pairs and revealed stable trait clusters, including a complex branch involving lipids with cardiovascular, autoimmune, and neuropsychiatric disorders. Furthermore, using a CRISPR-screen, we show that genes involved in lipid regulation exhibit more consistent trait associations through gene modules than individual genes. Our results suggest that a gene module perspective can contextualize genetic associations and prioritize alternative treatment targets when GWAS hits are not druggable.

Introduction

Human diseases have tissue-specific etiologies and manifestations [1,2,3]. In this context, determining how genes influence these complex phenotypes requires mechanistically understanding expression regulation across different cell types [4,5,6], which in turn should lead to improved treatments [7,8]. Previous studies have described regulatory DNA elements, including chromatin-state annotations [9,10], high-resolution enhancers [11,12], DNase I hypersensitivity maps [5], and genetic effects on gene expression across different tissues [4]. Integrating functional genomics data and GWAS data [13] has improved the identification of these transcriptional mechanisms that, when dysregulated, commonly result in tissue- and cell lineage-specific pathology.

Given the availability of gene expression data across several tissues [4,14,15,16], a popular approach to identify these biological processes is the transcription-wide association study (TWAS), which integrates expression quantitative trait loci (eQTLs) data to provide a mechanistic interpretation for GWAS findings. TWAS relies on testing whether perturbations in gene regulatory mechanisms mediate the association between genetic variants and human diseases [17,18,19,20]. However, TWAS have not reliably detected tissue-specific effects because eQTLs are commonly shared across tissues [21,22]. This sharing makes it challenging to identify the tissue or tissues specifically associated with a phenotype. Alternative existing statistical approaches that connect GWAS findings with gene expression data can infer disease-relevant tissues and cell types [22,23,24,25,26,27], but they generally rely on small sets of expression data compared with the total number of RNA-seq samples that are increasingly available [14,15]. Moreover, widespread gene pleiotropy and polygenic traits reveal the highly interconnected nature of transcriptional networks [28,29], where potentially all genes expressed in disease-relevant cell types have a non-zero effect [30,31]. Consequently, this complicates the interpretation of genetic effects and hampers translational efforts.

We propose PhenoPLIER, a polygenic approach that maps both gene-trait associations and drug-transcriptional responses into a common representation for a joint analysis. For this, we integrated more than 4,000 gene-trait associations (using TWAS from PhenomeXcan [32]) and transcriptional profiles of drugs (LINCS L1000 [33]) into a low-dimensional space learned from public gene

expression data on tens of thousands of RNA-seq samples (recount2 [14,34]). We used a latent representation defined by a computational approach [35] that learns recurrent gene co-expression patterns with certain sparsity constraints and preferences for those that align with prior knowledge (pathways). This low-dimensional space comprised features representing groups of genes (gene modules) with coordinated expression across different tissues and cell types. When mapping gene-trait associations to this reduced expression space, we observed that diseases were significantly associated with gene modules expressed in relevant cell types, such as hypothyroidism with T cells and thyroid, coronary artery disease with cardiomyocytes, hypertension and lipids with adipose tissue, and heart problems with heart ventricle and muscle cells. We replicated gene module associations with cardiovascular and autoimmune diseases in the Electronic Medical Records and Genomics (eMERGE) network phase III [36]. Moreover, we performed a CRISPR-screen to analyze lipid regulation in HepG2 cells and observed more consistent trait associations with modules than we observe with individual genes. Our approach was also robust in finding meaningful gene module-trait associations, even when individual genes involved in lipid metabolism did not reach genome-wide significance in lipid-related traits. Compared to a single-gene approach, our module-based method also better predicted FDA-approved drug-disease links by capturing tissue-specific pathophysiological mechanisms linked with the mechanism of action of drugs (e.g., niacin with cardiovascular traits via a known immune mechanism), suggesting that modules may provide a better means to examine drug-phenotype relationships than individual genes. Finally, exploring the phenotype-module space also revealed stable trait clusters associated with relevant tissues, including a complex branch involving lipids with cardiovascular, autoimmune, and neuropsychiatric disorders.

Results

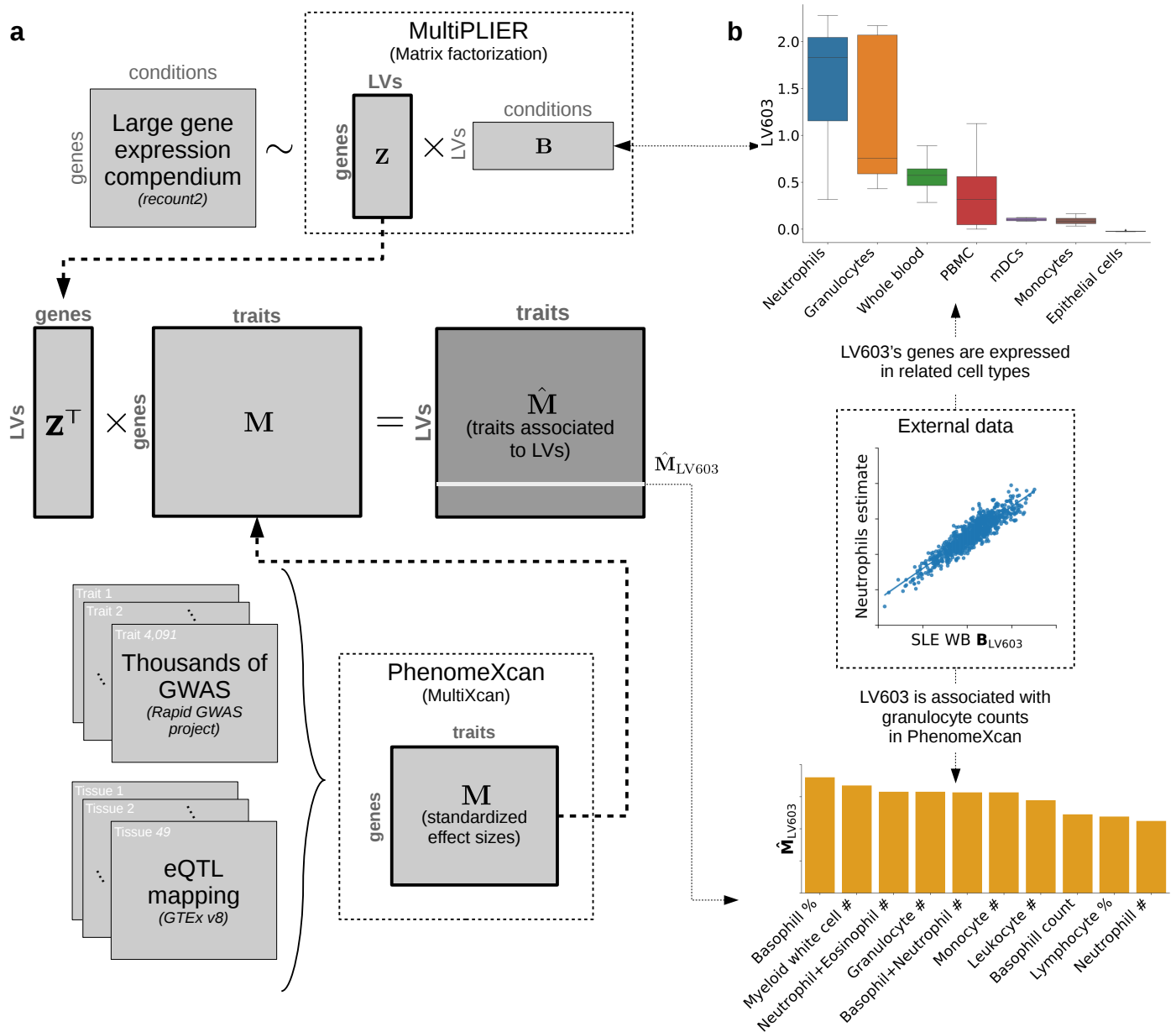## PhenoPLIER: an integration framework based on gene co-expression patterns

Figure 1: Schematic of the PhenoPLIER framework. a) The integration process between gene co-expression patterns from MultiPLIER (top) and TWAS results from PhenomeXcan (bottom). PhenoPLIER projects gene-trait associations to a latent space learned from large gene expression datasets. The process generates matrix $\hat{\mathbf{M}}$, where each trait is now described by latent variables (LV) or gene modules. **b)** After the integration process, we found that neutrophil counts and other white blood cells (bottom) were ranked among the top 10 traits for LV603, which was termed a neutrophil signature in the original MultiPLIER study. Genes in LV603 were expressed in relevant cell types (top). PBMC: peripheral blood mononuclear cells; mDCs: myeloid dendritic cells.

PhenoPLIER combines TWAS results with gene co-expression patterns by projecting gene-trait associations onto a latent gene expression representation (Figure 1). We used PhenomeXcan [32], a TWAS resource for the UK Biobank [37] and other cohorts that provides results for 4,091 different diseases and traits. We obtained a latent gene expression representation from MultiPLIER [34], an unsupervised learning approach applied to recount2 [14] (a gene expression dataset including RNA-seq data on a huge and heterogeneous number of samples, including rare diseases, cell types on specific differentiation stages, or under different stimuli, among others). Each of the 987 latent variables (LV) represents a gene module, essentially a group of genes with coordinated expression patterns (i.e., expressed together in the same tissues and cell types as a functional unit). Since LVs might represent a functional set of genes regulated by the same transcriptional program [38,39], the projection of TWAS results into this latent space could provide context for their interpretation. PhenoPLIER translates gene-trait associations to an LV-trait score, linking different traits and diseases to LVs representing specific cell types and tissues, even at specific developmental stages or under

distinct stimuli. Examining these LVs is possible because the MultiPLIER models link to samples, which may be annotated for experimental conditions (represented by matrix $\mathbf{B}$ in Figure 1 a) in which genes in an LV are expressed.

In the original MultiPLIER study, the authors found one of the latent variables, LV603, to be significantly associated with a known neutrophil pathway and highly correlated with neutrophil count estimates from gene expression [40]. We analyzed LV603 using PhenoPLIER (Figure 1 b) and found that neutrophil counts and other white blood cell traits were ranked among the top 10 traits for this LV, suggesting a high degree of internal consistency. We adapted the gene-property approach from MAGMA [41] for LVs and found that gene weights in this LV were predictive of gene associations for neutrophil abundance (FDR < 0.01). These initial results strongly suggested that shared patterns exist in the gene expression space (which has no GTEx samples) and the TWAS space (with gene models trained using GTEx v8); the approach linked transcriptional patterns from large and diverse dataset collections, including tissue samples and perturbation experiments, to complex traits.

LVs link genes that alter lipid accumulation with relevant traits and tissues

We performed a fluorescence-based CRISPR-Cas9 screen for genes associated with lipid accumulation. We found 271 genes associated with lipids accumulation by using a genome-wide lentiviral pooled CRISPR-Cas9 library targeting 19,114 genes in the human genome in the HepG2 cell line. From these, we identified two gene-sets that either caused a decrease (96 genes in total, with eight high-confidence genes: *BLCAP*, *FBXW7*, *INSIG2*, *PCYT2*, *PTEN*, *SOX9*, *TCF7L2*, *UBE2J2*) or an increase of lipids (175 genes in total, with six high-confidence genes: *ACACA*, *DGAT2*, *HILPDA*, *MBTPS1*, *SCAP*, *SRPR*) (Supplementary File 1). Four LVs were significantly enriched for these lipid-altering gene-sets (FDR<0.05) (Supplementary Table 1).

First, for each lipid-altering gene-set, we assessed the genes' effects on all phenotypes by adding their p-values (transformed to z-scores) and obtaining a ranked list of traits. The top associated traits for genes in the decreasing-lipids gene-set were highly relevant to lipid levels, such as hypertension, diastolic and systolic blood pressure, and vascular diseases, also including asthma and lung function (Supplementary Table 2). We performed the same operation for our LV-based approach by considering 24 LVs nominally enriched (unadjusted p-value < 0.05) with the decreasing-lipids gene-set by using Fast Gene Set Enrichment Analysis (FGSEA) [42]. In this case, we also found lipid-related traits among the top 25, including hypertension, blood pressure, cardiometabolic diseases like atherosclerosis, and celiac disease (Supplementary Table 3).
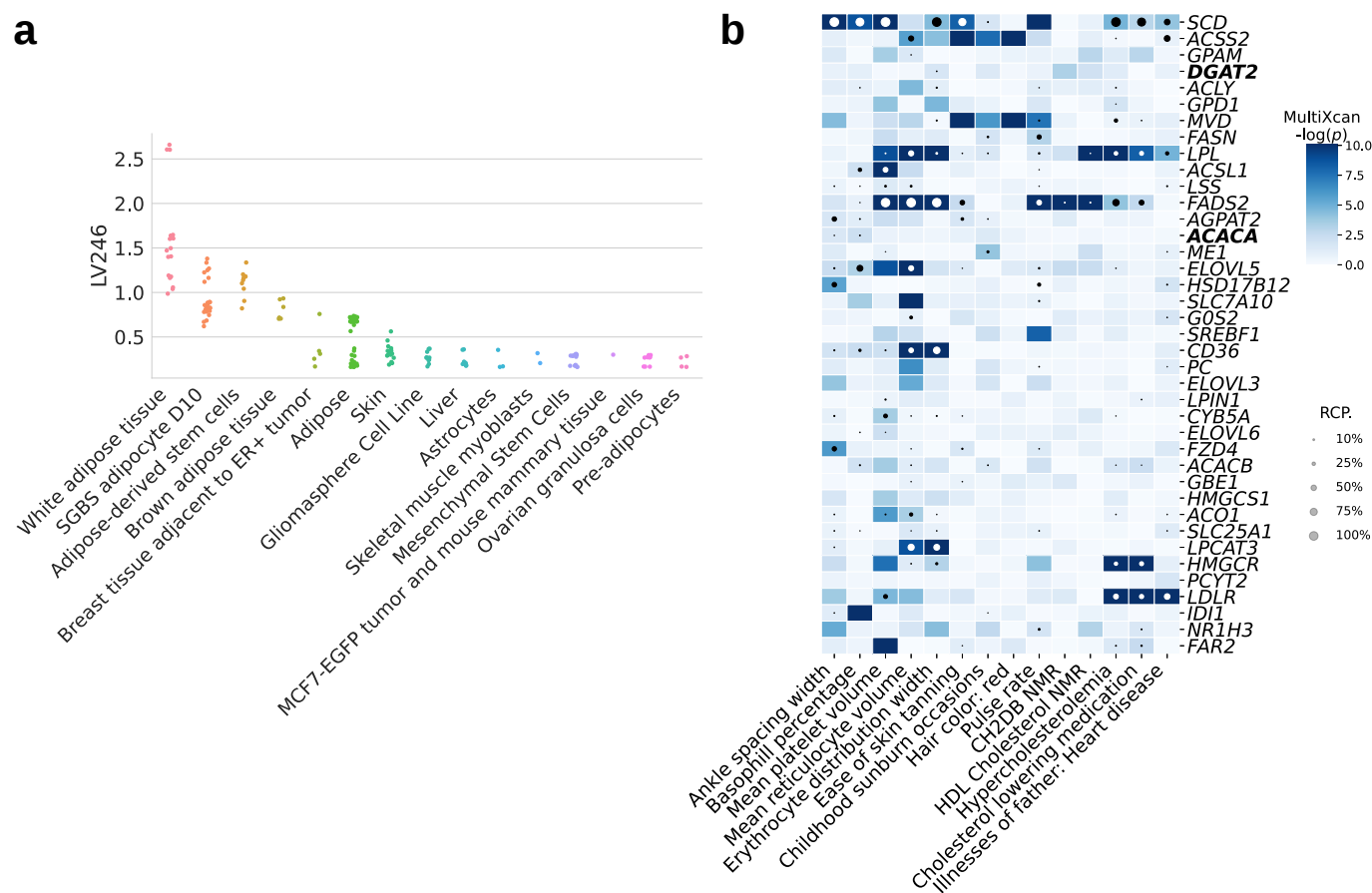
Figure 2: Tissues and traits associated with a gene module related to lipid metabolism (LV246). a) Top cell types/tissues where LV246's genes are expressed in. Values in the y-axis come from matrix **B** in the MultiPLIER models (Figure 1 a). In the x-axis, cell types/tissues are sorted by the maximum value. **b)** Gene-trait associations (S-MultiXcan; threshold at -log(p)=10) and colocalization probability (fastENLOC) for the top traits in LV246. The top 40 genes in LV246 are shown, sorted by their module weight, from largest (top gene *SCD*) to smallest (gene *FAR2*); *DGAT2* and *ACACA*, in bold, are two of the six high-confidence genes in the increasing-lipids gene set from our HepG2 CRISPR analyses. SGBS: Simpson Golabi Behmel Syndrome; CH2DB: CH$_2$ groups to double bonds ratio; NMR: nuclear magnetic resonance; HDL: high-density lipoprotein; RCP: locus regional colocalization probability.

When we considered the increasing-lipids gene-set, genes and LVs were associated with a more diverse set of traits, such as blood count tests, impedance measures, and bone-densitometry (Supplementary Tables 4 and 5). FGSEA found 27 LVs nominally enriched for the increasing-lipids gene-set which were associated with the same traits, and additionally to lung function, arterial stiffness, intraocular pressure, handgrip strength, rheumatoid arthritis, and celiac disease. Among these, LV246 contained genes mainly co-expressed in adipose tissue (Figure 2 a), which plays a key role in coordinating and regulating lipid metabolism. Additionally, using the gene-property analysis, we found that gene weights for this LV were predictive of gene associations for blood lipids and hypercholesterolemia (Supplementary Table 7). Two high-confidence genes from our CRISPR screening, *DGAT2* and *ACACA*, are responsible for encoding enzymes for triglycerides and fatty acid synthesis and were among the highest-weighted genes of LV246. However, as it can be seen in Figure 2 b, these two genes were not strongly associated with any of the top traits for this LV and thus would not be revealed by TWAS alone; other members of LV246, such as *SCD*, *LPL*, *FADS2*, *HMGCR*, and *LDLR*, were instead significantly associated and colocalized with lipid-related traits. This suggested that an LV-based perspective can integrate hits across modalities by leveraging information from functionally related genes.

PhenoPLIER with LVs predicts drug-disease pairs better than single genes

We systematically evaluated whether substituting LVs in place of individual genes more accurately predicted known treatment-disease pairs. For this, we used the transcriptional responses to small molecule perturbations profiled in LINCS L1000 [33], which were further processed and mapped to DrugBank IDs [43,44,45]. Based on an established drug repurposing strategy that matches reversed transcriptome patterns between genes and drug-induced perturbations [46,47], we adopted a previously described framework that uses imputed transcriptomes from TWAS to prioritize drug candidates [48]. For this, we computed a drug-disease score by anti-correlating the z-scores for a disease (from TWAS) and the z-scores for a drug (from LINCS) across sets of genes of different size. Therefore, a large score for a drug-disease pair indicated that a higher (lower) predicted expression of disease-associated genes are down (up)-regulated by the drug, thus predicting a potential treatment. Similarly, for the LV-based approach, we estimated how pharmacological perturbations affected the gene module activity by projecting expression profiles of drugs into our latent representation (see Methods). We used a manually-curated gold standard set of drug-disease medical indications [44,49] for 322 drugs across 53 diseases to evaluate the prediction performance.
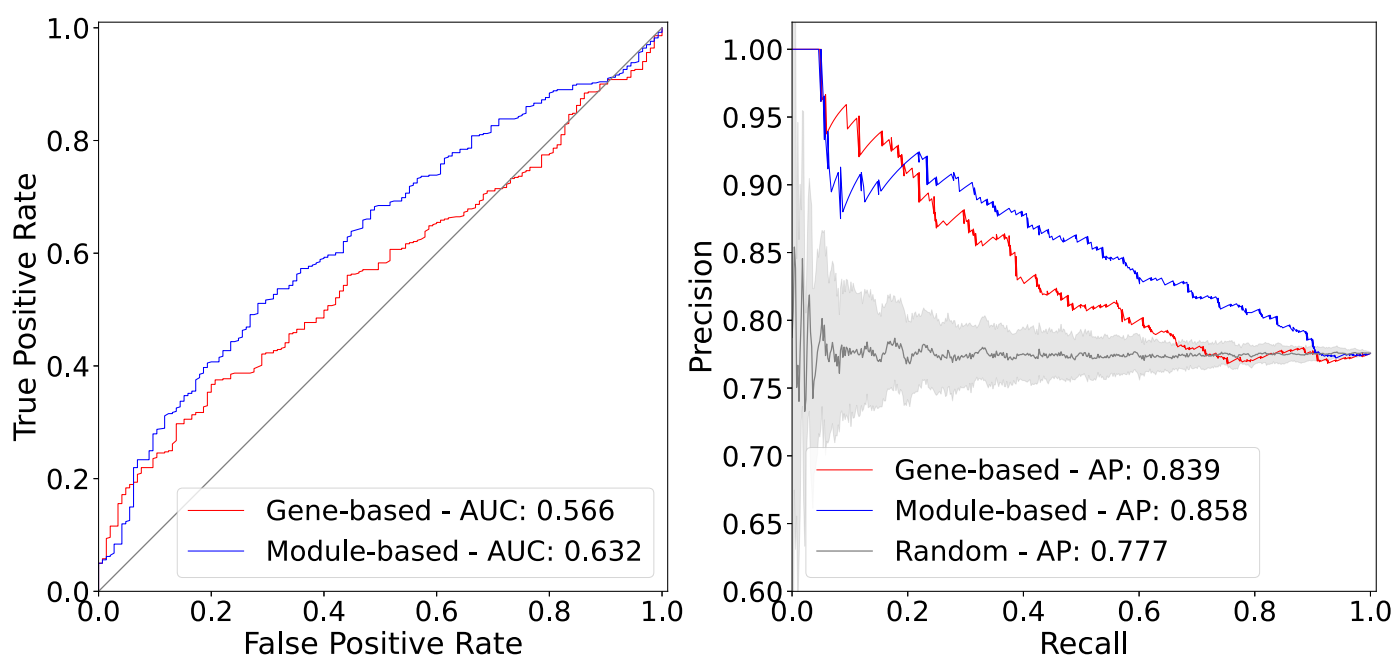

Figure 3: Drug-disease prediction performance for gene-based and module-based approaches. The receiver operating characteristic (ROC) (left) and the precision-recall curves (right) for a gene-based and our module-based approach. AUC: area under the curve; AP: average precision.

The gene-trait associations and drug-induced expression profiles projected into the latent space represent a compressed version of the entire set of results. Despite this compression, the LV-based method outperformed the gene-based one with an area under the curve of 0.632 and an average precision of 0.858 (Figure 3). The prediction results suggest that this low-dimensional space captures biologically meaningful patterns that can link pathophysiological processes with the mechanism of action of drugs.

We examined a specific drug-disease pair to determine whether the LVs driving the prediction were biologically plausible. Nicotinic acid (niacin) is a B vitamin widely used clinically to treat lipid disorders. Niacin exerts its effects on multiple tissues, although not all its mechanisms have been documented [50,51]. This compound can increase high-density lipoprotein (HDL) by inhibiting an HDL catabolism receptor in the liver. Niacin also inhibits diacylglycerol acyltransferase–2 (DGAT2), which decreases the production of low-density lipoproteins (LDL) by modulating triglyceride synthesis in hepatocytes, or by inhibiting adipocyte triglyceride lipolysis [50]. Niacin was one of the drugs in the gold standard indicated for atherosclerosis (AT) and coronary artery disease (CAD). For AT, the LV-based approach predicted niacin as a therapeutic drug with a score of 0.52 (above the mean), whereas the gene-based method assigned a negative score of -0.01 (below the mean). To understand why the LV-based

method gave an anticipated prediction different from the gene-based approach, we obtained the LVs that contributed substantially to the score, including those with top positive/negative LV values for the disease and top negative/positive LV values for the drug of interest. Notably, LV246 (analyzed previously) was among the top 20 modules contributing to the prediction of niacin as a therapeutic drug for AT. Gene weights of LV246 were predictive of cardiovascular traits (Supplementary Table 7), and several of its top genes were significantly associated and colocalized with cardiovascular-related traits: *SCD* (10q24.31) was associated with hypercholesterolemia (P=1.9e-5) and its GWAS and eQTL signals were fully colocalized (RCP=1.0); *LPL* (8p21.3), which was previously linked to different disorders of lipoprotein metabolism, was significantly associated with hypercholesterolemia (P=7.5e-17, RCP=0.26), and family history of heart disease (P=1.7e-5, RCP=0.22); other genes associated with hypercholesterolemia in this LV were *FADS2* (11q12.2) (P=9.42e-5, RCP=0.623), *HMGCR* (5q13.3) (P=1.3e-42, RCP=0.23), and *LDLR* (19p13.2) (P=9.9e-136, RCP=0.41).

The analysis of other niacin-AT-contributing LVs revealed additional known mechanisms of action of niacin. For example, *GPR109A/HCAR2* encodes a G protein-coupled high-affinity niacin receptor in adipocytes and immune cells, including monocytes, macrophages, neutrophils and dendritic cells [52,53]. It was initially thought that the antiatherogenic effects of niacin were solely due to inhibition of lipolysis in adipose tissue. However, it has been shown that nicotinic acid can reduce atherosclerosis progression independently of its antidyslipidemic activity through the activation of *GPR109A* in immune cells [54], thus boosting anti-inflammatory processes and reversing cholesterol transport [55]. In addition, flushing, a common adverse effect of niacin, is also produced by the activation of GPR109A in Langerhans cells (macrophages of the skin). This alternative mechanism for niacin could have been hypothesized by examining the cell types where the top two modules positively contributing to the niacin-AT prediction are expressed: LV116 and LV931 (Supplementary Figures 14 and 15). Among these, we also found LV678 positively contributing to this prediction, which was significantly enriched with the lipids-decreasing genes from our CRISPR screening (Supplementary Table 1). This module was expressed in the heart and muscle cells (Supplementary Figure 13).

The LV-based method was able to integrate different data types to provide an interpretable approach for drug repositioning research based on genetic studies. Additionally, our approach could also be helpful to understand better the mechanism of pharmacological effect of known or experimental drugs. For example, LV66, one of the top LVs affected by niacin (Supplementary Figure 16) was mainly expressed in ovarian granulosa cells. This compound has been very recently considered as a potential therapeutic for ovarian diseases [56,57], as it was found to promote follicle growth and inhibit granulosa cell apoptosis in animal models. Our LV-based approach could be helpful to generate novel hypotheses to evaluate potential mechanisms of action, or even adverse effects, of different drugs.

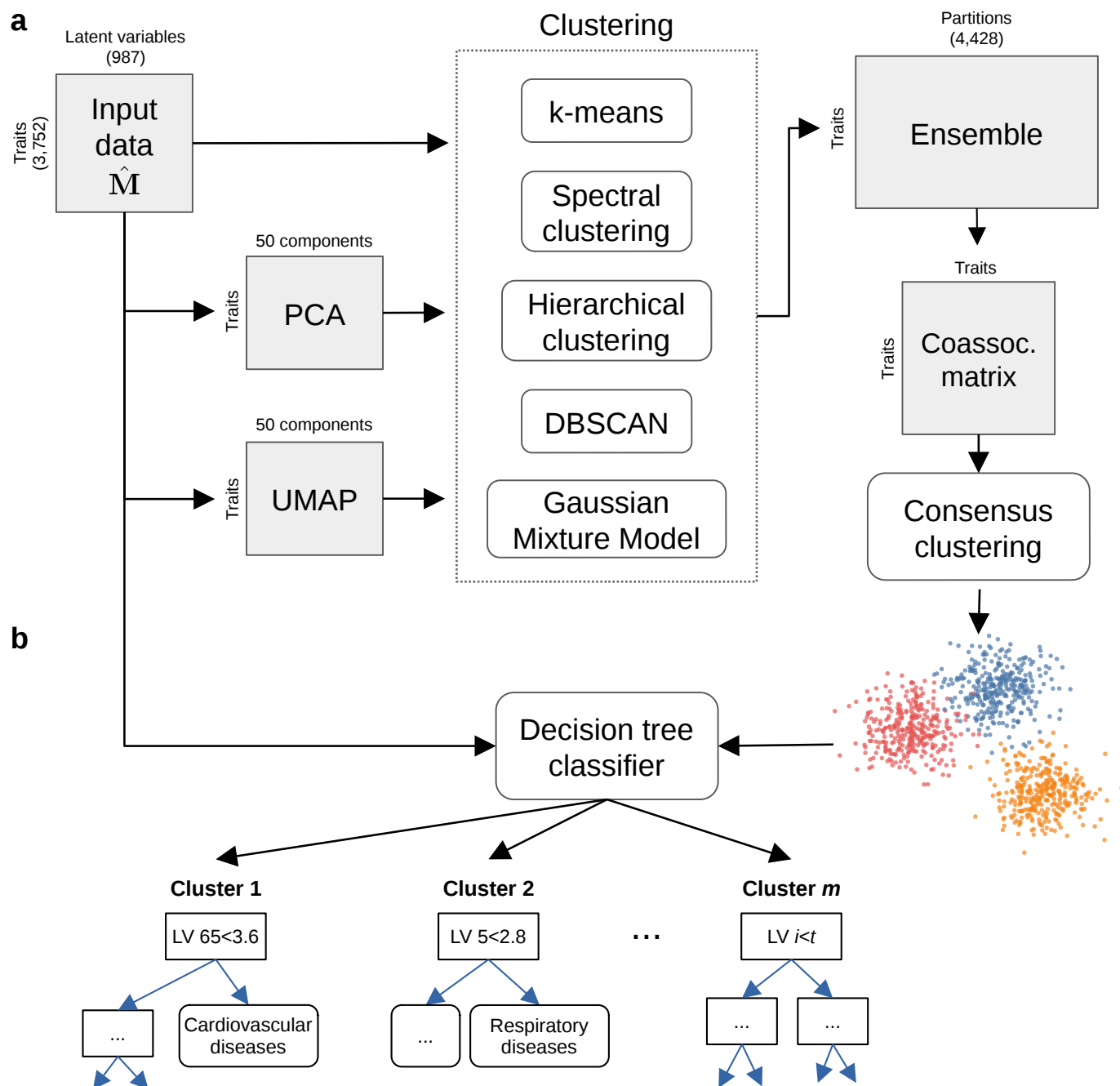## LV projections reveal trait clusters with shared transcriptomic properties

Figure 4: Cluster analysis on traits using the latent gene expression representation. a) The projection of TWAS results on n=3,752 traits into the latent gene expression representation is the input data to the clustering process. A linear (PCA) and non-linear (UMAP) dimensionality reduction techniques were applied to the input data, and the three data versions were processed by five different clustering algorithms. These algorithms derive partitions from the data using different sets of parameters (such as the number of clusters), leading to an ensemble of 4,428 partitions. Then, a distance matrix is derived by counting how many times a pair of traits were grouped in different clusters across the ensemble. Finally, a consensus function is applied to the distance matrix to generate consolidated partitions with different number of clusters (from 2 to $\sqrt{n} \approx 60$). These final solutions were represented in the clustering tree (Figure 5). **b)** The clusters found by the consensus function were used as labels to train a decision tree classifier on the original input data, which detects the LVs that better differentiate groups of traits.

The previous results suggested that the compression into $\hat{\mathbf{M}}$ increases the signal-to-noise ratio. Thus, we analyzed $\hat{\mathbf{M}}$ to find groups of traits that were affected by the same transcriptional processes. Selecting a clustering algorithm implies that a particular assumption about the structure of the data is most appropriate. Instead, we employed a consensus clustering approach where we applied different methods with varying sets of parameters and later combined these into a consolidated solution. Our clustering pipeline generated 15 final consensus clustering solutions with 5 to 29 clusters (Supplementary Figure 33). Instead of selecting a specific number of clusters, we used a clustering

tree [58] (Figure 5) to examine stable groups of traits across multiple resolutions. To interpret the clusters, we trained a decision tree classifier (a highly interpretable machine learning model) on the input data $\hat{\mathbf{M}}$ using the clusters found as labels. This quickly revealed the latent variables/gene modules that differentiated the groups of traits.
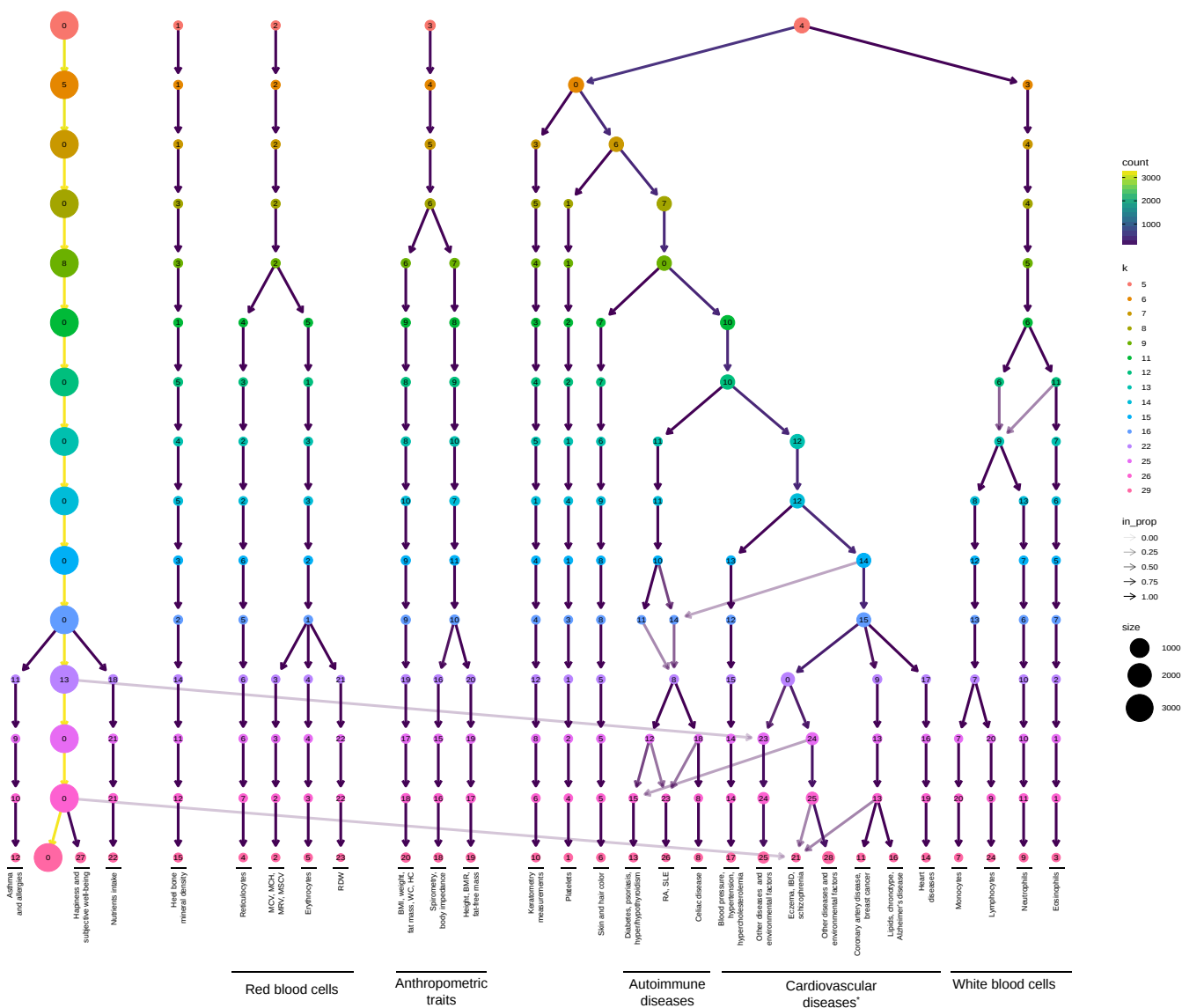

Figure 5: Clustering tree using multiple resolutions for clusters of traits. Each row represents a partition/grouping of the traits, and each circle is a cluster from that partition, and the number of clusters go from 5 to 29. Arrows indicate how traits in one cluster move across clusters from different partitions. Most of the clusters are preserved across different resolutions, showing highly stable solutions even with independent runs of the clustering algorithm. MCV: mean corpuscular volume; MCH: mean corpuscular hemoglobin; MRV: mean reticulocyte volume; MSCV: mean sphered cell volume; RDW: red cell (erythrocyte) distribution width; BMI: body mass index; WC: waist circumference; HC: hip circumference; BMR: basal metabolic rate; RA: rheumatoid arthritis; SLE: systemic lupus erythematosus; IBD: inflammatory bowel disease; *Descriptions of traits by cluster IDs (from left to right):* 12: also includes lymphocyte count and allergies such as allergic rhinitis or eczema; 4: includes reticulocyte count and percentage, immature reticulocyte fraction, and high light scatter reticulocytes count and percentage; 5: includes erythrocyte count, hemoglobin concentration, and hematocrit percentage; 18: also includes ankle spacing width; 1: includes platelet count, crit, mean volume, and distribution width; 13: diabetes refers to age when the diabetes was first diagnosed; 25: includes vascular problems such as angina, deep vein thrombosis (DVT), intraocular pressure, eye and mouth problems, pulse rate, hand-grip strength, several measurements of physical activity, jobs involving heavy physical work, types of transport used, intake of vitamin/mineral supplements, and various types of body pain and medications for pain relief; 21: also includes attention deficit hyperactivity disorder (ADHD), number of years of schooling completed, bone density, and intracranial volume measurement; 28: includes diabetes, gout, arthrosis, and respiratory diseases (and related medications such as ramipril, allopurinol, and lisinopril), urine assays, female-specific factors (age at menarche, menopause, first/last live birth), and several environmental/behavioral factors such as intake of a range of food/drink items including alcohol, time spent outdoors and watching TV, smoking and sleeping habits, early-life factors (breastfed as a baby, maternal

smoking around birth), education attainment, psychological and mental health, and health satisfaction; 11: also includes fasting blood glucose and insulin measurement; 16: lipids include high and low-density lipoprotein cholesterol (HDL and LDL), triglycerides, and average number of methylene groups per a double bond; 14: includes myocardial infarction, coronary atherosclerosis, ischaemic heart disease (wide definition). 9: includes neutrophil count, neutrophil+basophil count, neutrophil+eosinophil count, granulocyte count, leukocyte count, and myeloid cell count.

We found that phenotypes grouped into five clear branches (Figure 5). These were 0) a "large" branch that includes most of the traits subdivided only starting at k=16 (with asthma, subjective well-being traits, and nutrient intake clusters), 1) heel bone-densitometry measurements, 2) hematological assays on red blood cells, 3) physical measures, including spirometry and body impedance, and anthropometric traits with fat-free and fat mass measures in separate sub-branches, and 4) a "complex" branch including keratometry measurements, assays on white blood cells and platelets, skin and hair color traits, autoimmune disorders (type 1 diabetes, psoriasis, hyper/hypothyroidism, rheumatoid arthritis, systemic lupus erythematosus, celiac disease), and cardiovascular diseases (hypertension, coronary artery disease, myocardial infraction, hypercholesterolemia, and other cardiovascular-related traits such hand-grip strength [59], and environmental/behavioral factors such as physical activity and diet) (See Supplementary Files 1-5 for clustering results). Within these branches, results were relatively stable. The same traits were often clustered together across different resolutions, even with the consensus algorithm using random initializations at each level. Arrows between different clusters show traits moving from one group to another across different resolutions. This mainly happens between clusters within the "complex" branch, and between clusters from the "large" branch to the "complex" branch. We would expect that continuing to explore higher dimensionalities would result in further subdivisions of these large groupings. This behavior was expected since complex diseases are usually associated with shared genetic and environmental factors and are thus hard to categorize into a single cluster. We would also expect that exploring solutions with a larger number of clusters would result in further subdivisions of these large groupings.
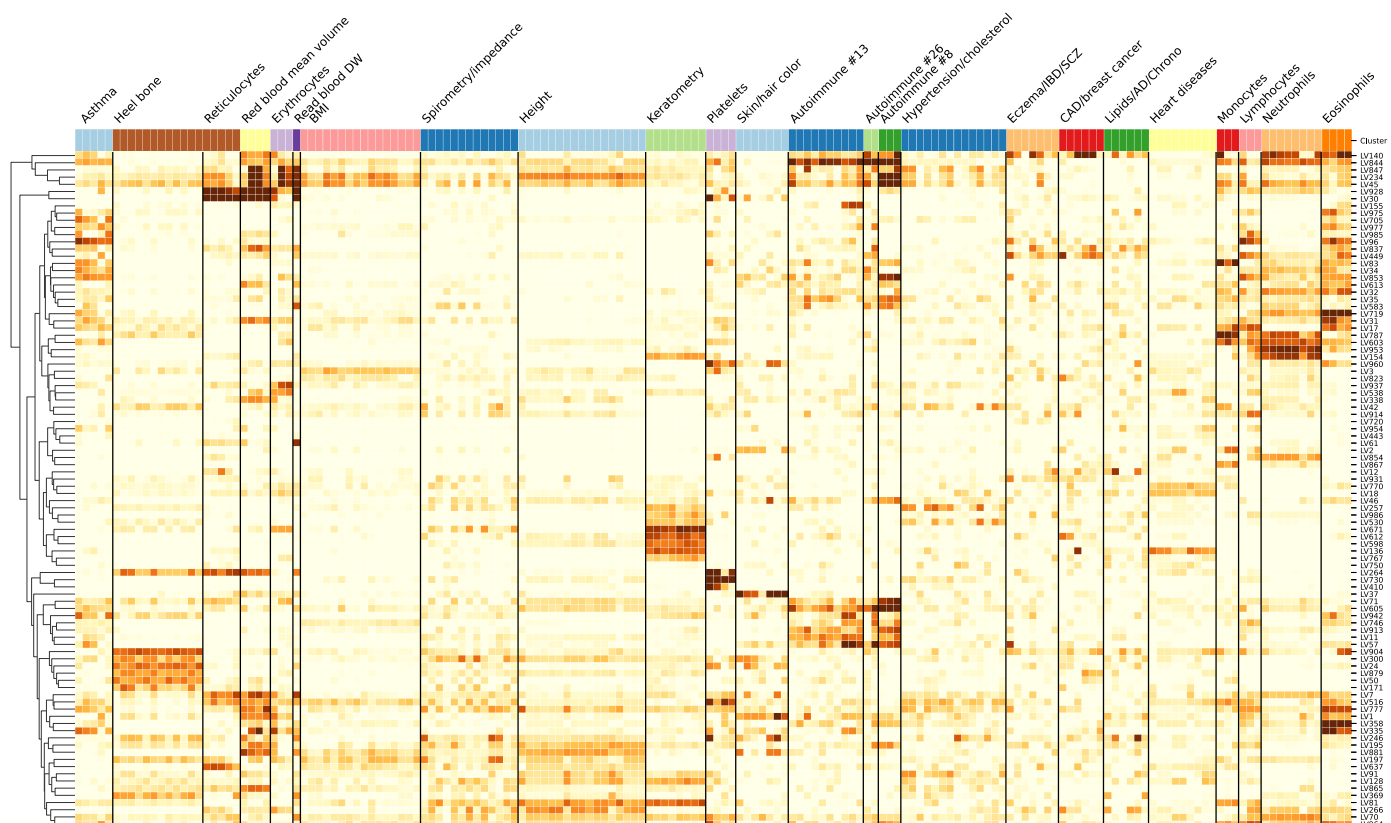

Figure 6: Cluster-specific and general transcriptional processes. The plot shows a submatrix of $\hat{\mathbf{M}}$ for the main trait clusters at k=29, considering only LVs (rows) that align well with at least one known pathway. Values are standardized from -5 (lighter color) to 16 (darker color).

Next, we analyzed which LVs were driving these clusters of traits. We trained decision tree classifiers on the input data (Figure 4) using each cluster at k=29 (bottom of Figure 5) as labels (see Methods). This yielded for each cluster the top LVs, where several of them were well-aligned to existing pathways, and others were "novel" and expressed in relevant tissues. We summarized this in Figure 6, where it can be seen that some LVs were highly specific to certain types of traits, while some were associated with a wide range of different traits and diseases, thus potentially involved in more general biological functions. For example, LVs such as LV928 and LV30 (Supplementary Figures 17 and 18), which were well-aligned to early progenitors of the erythrocytes lineage [60], were predominantly expressed in early differentiation stages of erythropoiesis, and strongly associated with different assays on red blood cells (erythrocytes and reticulocytes). On the other side, others, such as LV730, were highly specific and expressed in thrombocytes from different cancer samples (Supplementary Figures 19), and strongly associated with hematological assays on platelets; or LV598, whose genes were expressed in corneal endothelial cells (Supplementary Figures 20) and associated with keratometry measurements (FDR < 0.05; Supplementary Table 12).

The autoimmune diseases sub-branch also had significant LVs associations expressed in relevant cell types. LV155 was strongly expressed in thyroid (Supplementary Figures 21), and significantly associated with hypothyroidism both in PhenomeXcan and eMERGE (FDR < 0.05; Supplementary Tables 13 and 14). LV844 was the most strongly associated gene module with autoimmune disorders (FDR < 1e-15; Supplementary Tables 15 and 16), and was expressed in a wide range of cell types, including blood, breast organoids, myeloma cells, lung fibroblasts, and different cell types from the brain (Supplementary Figures 22). Other important LVs associated with autoimmunity in both PhenomeXcan and eMERGE were LV57 expressed in T cells (Supplementary Figure 23, and Supplementary Tables 17 and 18), and LV54 expressed in different soft tissue tumors, breast, lung, pterygia and epithelial cells (Supplementary Figure 24, and Supplementary Tables 19 and 20).

The cardiovascular sub-branch also exhibited significant associations, such as LV847 (Supplementary Figure 25) with blood pressure traits and hypertension (Supplementary Tables 21 and 22), which was expressed in CD19 (B cells) (which are related to preeclampsia [61]), Jurkat cells (T lymphocyte cells), and cervical carcinoma cell lines (the uterus was previously reported to be linked to blood pressure through a potential hormonal pathway [62,63]). LV136 was aligned with known collagen formation and muscle contraction pathways, and it was associated to coronary artery disease, myocardial infarction and keratometry measurements (Supplementary Tables 23 and 24), and expressed in a wide range of cell types, including fibroblasts, mesenchymal stem cells, osteoblasts, pancreatic stellate cells, cardiomyocytes, and adipocytes (Supplementary Figure 26). Lipids were clustered with chronotype and Alzheimer's disease, and were significantly associated with several modules expressed mainly in brain cell types, including LV93 (Supplementary Figure 27, and Supplementary Tables 25 and 26), LV206 (Supplementary Figure 28, and Supplementary Tables 27 and 28), and LV260 (Supplementary Figure 29, and Supplementary Tables 29 and 30). These modules were associated mainly with cardiovascular traits in eMERGE.

Within the cardiovascular sub-branch, we found neuropsychiatric and neurodevelopmental disorders such as Alzheimer's disease, schizophrenia, and attention deficit hyperactivity disorder (ADHD). These disorders were previously linked to the cardiovascular system [64,65,66,67], and share several risk factors, including hypertension, high cholesterol, obesity, smoking, among others [68,69]. In our results, however, these diseases were grouped by potentially shared transcriptional processes expressed in specific tissues/cell types. Alzheimer's disease, for example, was significantly associated with LV21 (FDR < 1e-18) and with LV5 (FDR < 0.01) (Supplementary Tables 31 and 33). LV21 was strongly expressed in a variety of soft tissue sarcomas, monocytes/macrophages (including microglia from cortex samples), and aortic valves (Supplementary Figure 30); as discussed previously, macrophages play a key role in the reverse cholesterol transport and thus atherogenesis [70]. LV5 was expressed in breast cancer and brain glioma samples, microglia (cortex), liver, and kidney, among other cell types (Supplementary Figure 31). LV21 and LV5 were also strongly associated with lipids:

LDL cholesterol (FDR < 0.001) and triglycerides (FDR < 0.05 and FDR < 0.001, respectively). Additionally, LV5 was associated with depression traits from the UK Biobank. ADHD was the only significantly associated trait for LV434 (FDR < 0.01) (Supplementary Table 35), which was expressed in breast cancer and glioma cells, cerebral organoids, and several different cell populations from the brain: fetal neurons (replicating and quiescence), microglia, and astrocytes (Supplementary Figure 32). Schizophrenia was not significantly associated with any gene module tested in our analysis. None of these LVs were aligned to prior pathways, which might represent potentially novel transcriptional processes affecting the cardiovascular and central nervous systems.

Discussion

We have introduced a novel computational approach that can map TWAS results into a representation learned from gene expression to infer cell type-specific features of complex phenotypes. Our key innovation is that we project association statistics through a representation and that representation is derived not strictly from measures of normal tissue but also cell types under a variety of stimuli and at various developmental stages. We found that this analysis using latent representations prioritized relevant associations, even when single gene-trait effects are not detected with standard methods. Projecting gene-trait and gene-drug associations into this common representation links drug-disease treatment pairs more accurately than the single-gene method we derived this strategy from; and the findings were more interpretable for potential mechanisms of action. Finally, we found that the analysis of associations through latent representations provided reasonable groupings of diseases and traits affected by the same transcriptional processes and highlighted disease-specific modules expressed in highly relevant tissues.

In some cases, the features linked to phenotypes appear to be associated with specific cell types. Associations with such cell type marker genes may reveal cell types that are potentially causal for a phenotype with more precision. We observed modules expressed primarily in one tissue (such as adipose in LV246, thyroid in LV155, or ovary in LV66). Others appeared to be expressed in many contexts. These may capture pathways associated with a set of related complex diseases (for example, LV136 is associated with coronary artery disease and keratometry measurements, and expressed in fibroblasts, osteoblasts, pancreas, liver, and cardiomyocytes). To our knowledge, projection through a representation learned on complementary but distinct datasets is a novel approach to identify cell type and pathway effects on complex phenotypes that is computationally simple to implement.

Our approach rests on the assumption that gene modules with coordinated expression will also manifest coordinated pathological effects. Our implementation in this work integrates two complementary approaches. One, MultiPLIER, which extracts latent variables from large expression datasets. In this case, we use a previously published model derived from the analysis of recount2, which was designed for interpretability. The MultiPLIER LVs could represent real transcriptional processes or technical factors ("batch effects"). Also, the underlying factorization method rests on linear combinations of variables, which could miss important and more complex co-expression patterns, and the training dataset of recount2 has since been surpassed in size and scale by other resources [15,71]. Second, TWAS have several limitations that can lead to false positives [72,73]. Like GWAS, which generally detects groups of associated variants in LD (linkage disequilibrium), TWAS usually identifies several genes within the same locus [20,74]. This is due to sharing of GWAS variants in gene expression models, to correlated expression of nearby genes, or even correlation of their predicted expression due to eQTLs in LD, among others [72]. Larger datasets and methods designed to learn representations with this application in mind could further refine the approach and are a promising avenue for future research.

Our findings are concordant with previous studies showing that drugs with genetic support are more likely to succeed through the drug development pipeline [7,48]. In this case, projecting association results through latent variables better prioritizes disease-treatment pairs than considering single-gene effects alone. An additional benefit is that the latent variables driving predictions can be examined. We also demonstrate that clustering trees, introduced as a means to examine developmental processes in single-cell data, provide multi-resolution grouping of phenotypes based on latent variable associations. In this portion, we used S-MultiXcan associations, which only provide the association strength between a gene and a trait, but with no direction of effect. This does mean that traits are grouped based on associated genes, but genes could have opposite effects on traits within the same cluster. Second, we employed hard-partitioning algorithms (one trait belongs exclusively to one cluster) where the distance between two traits takes into account all gene modules. Considering groups of related diseases was previously shown to be more powerful to detect shared genetic etiology [75,76], and clustering trees provide a way to explore such relationships in the context of latent variables.

Ultimately, the key to performance is the quality of the representations. Here we use a representation derived from a factorization of bulk RNA-seq data. Detailed perturbation datasets and single-cell profiling of tissues, with and without perturbagens, and at various stages of development provide an avenue to generate higher quality and more interpretable representations. The key to interpretability is driven by the annotation of sample metadata. New approaches to infer and annotate with structured metadata are promising and can be directly applied to existing data [77]. Rapid improvements in both areas set the stage for latent variable projections to be widely applied to disentangle the genetic basis of complex human phenotypes.

Methods

PhenomeXcan: gene-based associations on 4,091 traits

We used TWAS results from PhenomeXcan [32] on 4,091 traits for 22,515 genes. PhenomeXcan was built using publicly available GWAS summary statistics to compute 1) gene-based associations with the PrediXcan family of methods [19,20,78], and 2) a posterior probability of colocalization between GWAS loci and *cis*-eQTL with fastENLOC [32,79]. The PrediXcan family of methods first build prediction models using data from the Genotype-Tissue Expression project (GTEx v8) [4] for gene expression imputation and then correlate this predicted expression with the phenotype of interest. This family is comprised of S-PrediXcan [78] (which computes a gene-tissue-trait association using GWAS as input) and S-MultiXcan [19] (which computes a gene-trait association by aggregating evidence of associations across all tissues).

We refer to the standardized effect sizes (z-scores) of S-PrediXcan across n traits and m genes in tissue t as $\mathbf{M}^t \in \mathbb{R}^{n \times m}$. For S-MultiXcan we do not have the direction of effect, and we used the p-values converted to z-scores $\mathbf{M} = \Phi^{-1}(1 - p/2)$, where Φ^{-1} is the probit function. Higher z-scores correspond to stronger associations.

MultiPLIER and Pathway-level information extractor (PLIER)

MultiPLIER [34] extracts patterns of co-expressed genes from recount2 [14], a large gene expression dataset. The approach applies the pathway-level information extractor method (PLIER) [35], which performs unsupervised learning using prior knowledge (canonical pathways) to reduce technical noise. Via a matrix factorization approach, PLIER deconvolutes the gene expression data into a set of latent variables (LV), where each represents a gene module. This reduced the data dimensionality into 987 latent variables or gene modules.

Given a gene expression dataset $\mathbf{Y}^{m \times c}$ with m genes and c experimental conditions and a prior knowledge matrix $\mathbf{C} \in \{0, 1\}^{m \times p}$ for p MSigDB pathways [80] (so that $\mathbf{C}_{ij} = 1$ if gene i belongs to pathway j), PLIER finds $\mathbf{U}$, $\mathbf{Z}$, and $\mathbf{B}$ minimizing

$$||\mathbf{Y} - \mathbf{ZB}||_F^2 + \lambda_1||\mathbf{Z} - \mathbf{CU}||_F^2 + \lambda_2||\mathbf{B}||_F^2 + \lambda_3||\mathbf{U}||_{L^1} \tag{1}$$

subject to $\mathbf{U} > 0, \mathbf{Z} > 0$; $\mathbf{Z}^{m \times l}$ are the gene loadings with l latent variables, $\mathbf{B}^{l \times c}$ is the latent space for c conditions, $\mathbf{U}^{p \times l}$ specifies which of the p prior-information pathways in $\mathbf{C}$ are represented for each LV, and λ_i are different regularization parameters used in the training step. $\mathbf{Z}$ is a low-dimensional representation of the gene space where each LV aligns as much as possible to prior knowledge, and it might represent either a known or novel gene module (i.e., a meaningful biological pattern) or noise.

We projected $\mathbf{M}$ (either from S-PrediXcan across each tissue, or S-MultiXcan) into the low-dimensional gene module space learned by MultiPLIER using:

$$\hat{\mathbf{M}} = (\mathbf{Z}^\top \mathbf{Z} + \lambda_2 \mathbf{I})^{-1} \mathbf{Z}^\top \mathbf{M}. \tag{2}$$

where in $\hat{\mathbf{M}}^{l \times n}$ all traits in PhenomeXcan are now described by gene modules.

Gene module-trait associations

To compute an association between a gene module and a trait, we used an approach similar to the gene-property analysis in MAGMA [41], which is essentially a competitive test using gene weights from $\mathbf{Z}$ to predict gene z-scores from $\mathbf{M}$. Thus, the regression model uses genes as data points by fitting $\mathbf{m} = \beta_0 + \mathbf{z}\beta_z + \epsilon$, where $\epsilon \sim \mathrm{MVN}(0, \hat{\Sigma})$, $\mathbf{m}$ are gene p-values (for a trait) from S-MultiXcan that we transformed to z-scores as mentioned before. Since we are only interested in whether genes with a stronger membership to a module (highest weights) are more associated with the phenotype, we performed a one-sided test on the coefficient β_z with the null hypothesis of $\beta_z = 0$ against the alternative $\beta_z > 0$. Since the error terms ϵ could be correlated due to correlation between predicted expression, we used a generalized least squares approach instead of standard linear regression. To calculate $\hat{\Sigma}$, we first estimated the correlation of predicted expression for each gene pair $(\mathbf{t}_i, \mathbf{t}_j)$ in tissue t using equations from [19,78]:

$$
\begin{aligned}
\hat{\Sigma}_{ij}^t &= Cor(\mathbf{t}_i, \mathbf{t}_j) \\
&= \frac{Cov(\mathbf{t}_i, \mathbf{t}_j)}{\sqrt{\widehat{\mathrm{var}}(\mathbf{t}_i)\widehat{\mathrm{var}}(\mathbf{t}_j)}} \\
&= \frac{Cov(\sum_{a\in\mathrm{model}_i} w_a^i X_a, \sum_{b\in\mathrm{model}_j} w_b^j X_b)}{\sqrt{\widehat{\mathrm{var}}(\mathbf{t}_i)\widehat{\mathrm{var}}(\mathbf{t}_j)}} \\
&= \frac{\sum_{\substack{a\in\mathrm{model}_i \\ b\in\mathrm{model}_j}} w_a^i w_b^j Cov(X_a, X_b)}{\sqrt{\widehat{\mathrm{var}}(\mathbf{t}_i)\widehat{\mathrm{var}}(\mathbf{t}_j)}} \\
&= \frac{\sum_{\substack{a\in\mathrm{model}_i \\ b\in\mathrm{model}_j}} w_a^i w_b^j \Gamma_{ab}}{\sqrt{\widehat{\mathrm{var}}(\mathbf{t}_i)\widehat{\mathrm{var}}(\mathbf{t}_j)}},
\end{aligned}
\tag{3}
$$

where $\Gamma = \widehat{\mathrm{var}}(\mathbf{X}) = (\mathbf{X} - \bar{\mathbf{X}})^\top (\mathbf{X} - \bar{\mathbf{X}})/(m-1)$ is the genotype covariance matrix using 1000 Genomes Project data [81, 82]. The variances for predicted gene expression of gene i is estimated as:

$$
\begin{aligned}
\widehat{\mathrm{var}}(\mathbf{t}_i) &= (\mathbf{W}^i)^\top \Gamma^i \mathbf{W}^i \\
&= \sum_{\substack{a\in\mathrm{model}_i \\ b\in\mathrm{model}_i}} w_a^i w_b^i \Gamma_{ab}^i.
\end{aligned}
\tag{4}
$$

Finally, $\hat{\Sigma} = \sum_t \hat{\Sigma}^t / |t|$ where $|t|=49$ is the number of tissues.

Drug-disease prediction

For the drug-disease prediction, we used a method based on a drug repositioning framework previously used for psychiatry traits [48] where gene-trait associations are anticorrelated with expression profiles for drugs. For the single-gene approach, we computed a drug-disease score by multiplying each S-PrediXcan set of results in tissue t, $\mathbf{M}^t$, with the transcriptional responses profiled in LINCS L1000 [33], $\mathbf{L}^{c\times m}$ (for c compounds): $\mathbf{D}^{t,k} = -1 \cdot \mathbf{M}^{t,k}\mathbf{L}^\top$, where k refers to the number of most significant gene associations in $\mathbf{M}^t$ for each trait. As suggested in [48], k could be either all genes or the top 50, 100, 250, and 500; then we average score ranks across all k and obtain $\mathbf{D}^t$. Finally, for each drug-disease pair, we took the maximum prediction score across all tissues: $\mathbf{D}_{ij} = \max\{\mathbf{D}_{ij}^t \mid \forall t\}$.

The same procedure was used for the gene module-based approach, where we projected S-PrediXcan results into our latent representation, leading to $\hat{\mathbf{M}}^t$; and also $\mathbf{L}$, leading to $\hat{\mathbf{L}}^{l\times c}$. Finally, $\mathbf{D}^{t,k} = -1 \cdot \hat{\mathbf{M}}^{t,k}\hat{\mathbf{L}}^\top$, where in this case k could be all LVs or the top 5, 10, 25 and 50 (since have an order of magnitude less LVs than genes).

Since the gold standard of drug-disease medical indications used contained Disease Ontology IDs (DOID) [83], we mapped PhenomeXcan traits to the Experimental Factor Ontology [84] using [85], and then to DOID.

Consensus clustering of traits

We performed two preprocessing steps on the S-MultiXcan results before the cluster analysis procedure. First, we combined results in $\mathbf{M}$ (S-MultiXcan) for traits that mapped to the same Experimental Factor Ontology (EFO) [84] term using the Stouffer's method: $\sum w_i M_{ij}/\sqrt{\sum w_i^2}$, where w_i is a weight based on the GWAS sample size for trait i, and M_{ij} is the z-score for gene j. Second, we standardized all z-scores for each trait i by their sum to reduce the effect of highly polygenic traits: $M_{ij}/\sum M_{ij}$. Finally, we projected this data matrix using Equation 2, obtaining $\hat{\mathbf{M}}$ with n=3752 traits and l=987 LVs as the input of our clustering pipeline.

A partitioning of $\hat{\mathbf{M}}$ with n traits into k clusters is represented as a label vector $\pi \in \mathbb{N}^n$. Consensus clustering approaches consist of two steps: 1) the generation of an ensemble Π with r partitions of the dataset: $\Pi = \{\pi_1, \pi_2, \ldots, \pi_r\}$, and 2) the combination of the ensemble into a consolidated solution defined as:

$$\pi^* = \arg \max_{\hat{\pi}} Q(\{|\mathcal{L}^i|\phi(\hat{\pi}_{\mathcal{L}^i}, \pi_{i\mathcal{L}^i}) \mid i \in \{1, \ldots, r\}\}), \tag{5}$$

where $\mathcal{L}^i$ is a set of data indices with known cluster labels for partition i, $\phi \colon \mathbb{N}^n \times \mathbb{N}^n \to \mathbb{R}$ is a function that measures the similarity between two partitions, and Q is a measure of central tendency, such as the mean or median. We used the adjusted Rand index (ARI) [86] for ϕ, and the median for Q. To obtain π^*, we define a consensus function $\Gamma \colon \mathbb{N}^{n \times r} \to \mathbb{N}^n$ with Π as the input. We used consensus functions based on the evidence accumulation clustering (EAC) paradigm [87], where Π is first transformed into a distance matrix $\mathbf{D}_{ij} = d_{ij}/r$, where d_{ij} is the number of times traits i and j were grouped in different clusters across all r partitions in Π. Then, Γ can be any similarity-based clustering algorithm, which is applied on $\mathbf{D}$ to derive the final partition π^*.

For the ensemble generation step, we used different algorithms to create a highly diverse set of partitions (see Figure 4), since diversity is an important property for ensembles [88,89,90]. We used three data representations: the raw dataset, its projection into the top 50 principal components, and the embedding learned by UMAP [91] using 50 components. For each of these, we applied five clustering algorithms, covering a wide range of different assumptions on the data structure: k-means [92], spectral clustering [93], a Gaussian mixture model (GMM), hierarchical clustering, and DBSCAN [94]. For k-means, spectral clustering and GMM, we specified a range of k between 2 and $\sqrt{n} \approx 60$, and for each k we generated five partitions using random seeds. For hierarchical clustering, for each k we generated four partitions using four common linkage criteria: ward, complete, average and single. For DBSCAN, we combined different ranges for parameters ϵ (the maximum distance between two data points to be considered part of the same neighborhood) and $minPts$ (the minimum number of data points in a neighborhood for a data point to be considered a core point). Specifically, we used $minPts$ values from 2 to 125, and for each data version, we determined a plausible range of ϵ values by observing the distribution of the mean distance of the $minPts$-nearest neighbors across all data points. Since some combinations of $minPts$ and ϵ might not produce a meaningful partition (for instance, when all points are detected as noisy or only one cluster is found), we resampled partitions generated by DBSCAN to ensure an equal representation in the ensemble. This procedure generated a final ensemble of 4428 partitions.

Finally, we used spectral clustering on $\mathbf{D}$ to derive the final consensus partitions. $\mathbf{D}$ was first transformed into a similarity matrix by applying an RBF kernel $\exp(-\gamma \mathbf{D}^2)$ using four different values for γ that we empirically determined to work best. Thus for each k between 2 and 60, we derived four consensus partitions and selected the one that maximized Equation 5. We further filtered this set of

59 solutions to keep only those with an ensemble agreement larger than the 75th percentile, leaving a total of 15 final consensus partitions shown in Figure 5.

Cluster interpretation

We used a supervised learning approach to interpret clustering results by detecting which gene modules are the most important for clusters of traits. For this, we used the highest resolution partition (k=29, although any could be used) to train a decision tree model using each of the clusters as labels and the projected data $\hat{\mathbf{M}}$ as the training samples. For each k, we built a set of binary labels with the current cluster's traits as the positive class and the rest of the traits as the negative class. Then, we selected the LV in the root node of the trained model only if its threshold was positive and larger than one standard deviation. Next, we removed this LV from $\hat{\mathbf{M}}$ (regardless of being previously selected or not) and trained the model again. We repeated this procedure 20 times to extract the top 20 LVs that better discriminate traits in a cluster from the rest.

CRISPR-Cas9 screening

Cell culture. HepG2 cells were obtained from ATCC (ATCC® HB-8065™), and main-tained in Eagle's Minimum Essential Medium with L-Glutamine (EMEM, Cat. 112-018-101, Quality Biology) supplemented with 10% Fetal Bovine Serum (FBS, Gibco, Cat.16000-044), and 1% Pen/Strep (Gibco, Cat.15140-122). Cells were kept at 37oC in a humidity-controlled incubator with 5% CO2, and were maintained at a density not exceed more than 80% confluency.

Genome-wide lentiviral pooled CRISPR-Cas9 library. 3rd lentiviral generation, Broad GPP genome-wide Human Brunello CRISPR knockout Pooled library was provided by David Root and John Doench from Addgene (Cat. 73179-LV), and was used for HepG2 cell transduction. It consists of 76,441 sgRNAs, targets 19,114 genes in the human genome with an average of 4 sgRNAs per gene. Each 20nt sgRNA cassette was inserted into lentiCRIS-PRv2 backbone between U6 promoter and gRNA scaffold. Through cell transduction, the lentiviral vectors which encode Cas9 were used to deliver the sgRNA cassette containing plasmids into cells during cell replication. Unsuccessful transduced cells were excluded through puromycin selection.

Lentiviral titer determination. No-spin lentiviral transduction was utilized for the screen. In a Collagen-I coated 6-wells plate, approximate 2.5 M cells were seeded each well in the presence of 8ug/ml polybrene (Millipore Sigma, Cat. TR-1003 G), and a different titrated virus volume (e.g., 0, 50, 100, 200, 250, and 400ul) was assigned to each well. EMEM complete media was added to make the final volume of 1.24ml. 16-18hrs post transduction, virus/polybrene containing media was removed from each well. Cells were washed twice with 1x DPBS, and replaced with fresh EMEM. At 24h, cells in each well were trypsinized, diluted (e.g.,1:10), and seeded in pairs of wells of 6-well plates. At 60hr post transduction, cell media in each well was replaced with fresh EMEM. 2ug/ml of puromycin (Gibco, Cat. A1113803) was added to one well out of the pair. 2-5 days after puromycin selection, or the 0 virus well treated with puromycin had no survival of cells, cells in both wells with/without puromycin were collected and counted for viability. Percentage of Infection (PI%) was obtained by comparing the cell numbers with/without puromycin selection within each pair. By means of Poisson's distribution theory, when transduction efficiency (PI%) is between 30-50%, which corresponding to a MOI (Multiplicity of Infection) of ~0.35-0.70. At MOI equal or close to 0.3, around 95% of infected cells are predicted to have only one copy of virus. Therefore, a volume of virus (120ul) yielding 30-40% of transduction effi-ciency was chosen for further large-scale viral transduction.

Lentiviral Transduction in HepG2 Using Brunello CRISPR Knockout Pooled Library. In order to achieve a coverage (representation) of at least 500 cells per sgRNA, and at a MOI between 0.3-0.4 to ensure 95% of infected cells get only one viral particle per cell, ~200M cells were initiated for the

screen. Transduction was carried out in the similar fashion as de-scribed above. Briefly, 2.5M cells were seeded in each well of 14 6-well plates, along with 8ug/ml of polybrene. Volume of 120ul of virus was added to each experimental well. 18hrs post transduction, virus/PB mix medium was removed, and cells in each well were collect-ed, counted, and pooled into T175 flasks. At 60hr post transduction, 2ug/ml of puromycin was added to each flask. Mediums were changed every 2 days with fresh EMEM, topped with 2ug/ml puromycin. 7 days after puromycin selection, cells were collected, pooled, counted, and replated.

Fluorescent dye staining. 9 days after puromycin selection, cells were assigned to 2 groups. 20-30M cells were collected as Unsorted Control. Cell pellet was spun down at 500 x g for 5min at 4oC. Dry pellet was kept at -80oC for further genomic DNA isolation. The rest of the cells (approximately 200M) were kept in 100mm dishes, and stained with fluo-rescent dye (LipidSpotTM 488, Biotium, Cat. 70065-T). In Brief, LipidSpot 488 was diluted to 1:100 with DPBS. 4ml of staining solution was used for each dish, and incubated at 37oC for 30min. Cell images were captured through fluorescent microscope EVOS for GFP signal detection (Supplementary Figure 7).

Fluorescence-activated cell sorting (FACS). Cells were immediately collected into 50ml tubes (From this point on, keep cells cold), and spin at 500 x g for 5min at 4oC. After DPBS wash, cell pellets were resuspended with FACS Sorting Buffer (1x DPBS without Ca2+/Mg2+, 2.5mM EDTA, 25mM HEPES, 1% BSA. Solution was filter sterilized, and kept at 4oC), pi-pet gently to make single cells. Cell solution then filtered through cell strainer (Falcon, Cat. 352235), and were kept on ice protected from light. Collected cells were sorted on FACSJazz. 100um nozzle was used for sorting. ~20% of each GFP-High and GFP-Low (Supplementary Figure 8) were collected into 15ml tubes. After sorting, cells were immediately spun down. Pellets were kept in -80oC for further genomic DNA isolation.

Genomic DNA isolation and verification. 3 conditions of Genomic DNA (Un-Sorted Con-trol, lentiV2 GFP-High, and lentiV2 GFP-Low) were extracted using QIAamp DNA Blood Mini Kit (Qiagen, Cat.51104), followed by UV Spectroscopy (Nanodrop) to access the quality and quantity of the gDNA. Total 80-160ug of gDNA was isolated for each condi-tion. sgRNA cassette and lentiviral specific transgene in isolated gDNA were verified through PCR (Supplementary Figure 9).

Illumina libraries generation and sequencing. Fragment containing sgRNA cassette was amplified using P5 /P7 primers, as indicated in [95] and primer sequences were adapted from Broad Institute protocol (Supplementary Figure 10). Stagger sequence (0-8nt) was included in P5, and 8bp uniquely barcoded sequence in P7. Primers were syn-thesized through Integrated DNA Technologies (IDT), each primer was PAGE purified. 32 PCR reactions were set up for each condition. Each 100ul PCR reaction consists of roughly 5ug of gDNA, 5ul of each 10uM P5 and P7. ExTaq DNA Polymerase (TaKaRa, Cat. RR001A) was used to amplify the amplicon. PCR Thermal Cycler Parameters set as: Initial at 95oC for 1min; followed by 24 cycles of Denaturation at 94oC for 30 seconds, Annealing at 52.5oC for 30 seconds, Extension at 72oC for 30 seconds. A final Elongation at 72oC for 10 minutes. 285bp-293bp PCR products were expected (Supplementary Figure 11 A). PCR products within the same condition were pooled and purified using SPRIselect beads (Beckman Coulter, Cat. B23318). Purified illumina libraries were quantitated on Qubit, and the quality of the library were analyzed on Bio-analyzer using High Sensitivity DNA Chip. A single approxi-mate 285bp peak was expected. (Supplementary Figure 11 B). Final illumina library samples were se-quenced on Nova-seq 6000. Samples were pooled and loaded on a SP flow cell, along with 20% PhiX control v3 library spike-in.

References

1. **Relaxed purifying selection and possibly high rate of adaptation in primate lineage-specific genes.**
   James J Cai, Dmitri A Petrov
   Genome biology and evolution (2010-07-12) https://www.ncbi.nlm.nih.gov/pubmed/20624743
   DOI: 10.1093/gbe/evq019 · PMID: 20624743 · PMCID: PMC2997544

2. **Elevated rates of protein secretion, evolution, and disease among tissue-specific genes.**
   Eitan E Winter, Leo Goodstadt, Chris P Ponting
   Genome research (2004-01) https://www.ncbi.nlm.nih.gov/pubmed/14707169
   DOI: 10.1101/gr.1924004 · PMID: 14707169 · PMCID: PMC314278

3. **A large-scale analysis of tissue-specific pathology and gene expression of human disease genes and complexes**
   K. Lage, N. T. Hansen, E. O. Karlberg, A. C. Eklund, F. S. Roque, P. K. Donahoe, Z. Szallasi, T. S. Jensen, S. Brunak
   Proceedings of the National Academy of Sciences (2008-12-22) https://doi.org/d5qcv9
   DOI: 10.1073/pnas.0810772105 · PMID: 19104045 · PMCID: PMC2606902

4. **The GTEx Consortium atlas of genetic regulatory effects across human tissues**
   The GTEx Consortium
   Science (2020-09-11) https://doi.org/ghbnhr
   DOI: 10.1126/science.aaz1776 · PMID: 32913098 · PMCID: PMC7737656

5. **Index and biological spectrum of human DNase I hypersensitive sites**
   Wouter Meuleman, Alexander Muratov, Eric Rynes, Jessica Halow, Kristen Lee, Daniel Bates, Morgan Diegel, Douglas Dunn, Fidencio Neri, Athanasios Teodosiadis, … John Stamatoyannopoulos
   Nature (2020-07-29) https://doi.org/gg6dhp
   DOI: 10.1038/s41586-020-2559-3 · PMID: 32728217 · PMCID: PMC7422677

6. **Mechanisms of tissue and cell-type specificity in heritable traits and diseases**
   Idan Hekselman, Esti Yeger-Lotem
   Nature Reviews Genetics (2020-01-08) https://doi.org/ggkx9v
   DOI: 10.1038/s41576-019-0200-9 · PMID: 31913361

7. **The support of human genetic evidence for approved drug indications**
   Matthew R Nelson, Hannah Tipney, Jeffery L Painter, Judong Shen, Paola Nicoletti, Yufeng Shen, Aris Floratos, Pak Chung Sham, Mulin Jun Li, Junwen Wang, … Philippe Sanseau
   Nature Genetics (2015-06-29) https://doi.org/f3mn52
   DOI: 10.1038/ng.3314 · PMID: 26121088

8. **Are drug targets with genetic support twice as likely to be approved? Revised estimates of the impact of genetic support for drug mechanisms on the probability of drug approval**
   Emily A. King, J. Wade Davis, Jacob F. Degner
   PLOS Genetics (2019-12-12) https://doi.org/gg957r
   DOI: 10.1371/journal.pgen.1008489 · PMID: 31830040 · PMCID: PMC6907751

9. **An integrated encyclopedia of DNA elements in the human genome**
   The ENCODE Project Consortium

Nature (2012-09-05) https://doi.org/bg9d
DOI: 10.1038/nature11247 · PMID: 22955616 · PMCID: PMC3439153

10. **Integrative analysis of 111 reference human epigenomes**
Anshul Kundaje, Wouter Meuleman, Jason Ernst, Misha Bilenky, Angela Yen, Alireza Heravi-Moussavi, Pouya Kheradpour, Zhizhuo Zhang, Jianrong Wang, Michael J. Ziller, … Roadmap Epigenomics Consortium
Nature (2015-02-18) https://doi.org/f62jpn
DOI: 10.1038/nature14248 · PMID: 25693563 · PMCID: PMC4530010

11. **An atlas of active enhancers across human cell types and tissues**
Robin Andersson, Claudia Gebhard, Irene Miguel-Escalada, Ilka Hoof, Jette Bornholdt, Mette Boyd, Yun Chen, Xiaobei Zhao, Christian Schmidl, Takahiro Suzuki, … The FANTOM Consortium
Nature (2014-03-26) https://doi.org/r35
DOI: 10.1038/nature12787 · PMID: 24670763 · PMCID: PMC5215096

12. **Regulatory genomic circuitry of human disease loci by integrative epigenomics**
Carles A. Boix, Benjamin T. James, Yongjin P. Park, Wouter Meuleman, Manolis Kellis
Nature (2021-02-03) https://doi.org/ghzkhr
DOI: 10.1038/s41586-020-03145-z · PMID: 33536621 · PMCID: PMC7875769

13. **The Post-GWAS Era: From Association to Function**
Michael D. Gallagher, Alice S. Chen-Plotkin
The American Journal of Human Genetics (2018-05) https://doi.org/gdmftd
DOI: 10.1016/j.ajhg.2018.04.002 · PMID: 29727686 · PMCID: PMC5986732

14. **Reproducible RNA-seq analysis using recount2**
Leonardo Collado-Torres, Abhinav Nellore, Kai Kammers, Shannon E Ellis, Margaret A Taub, Kasper D Hansen, Andrew E Jaffe, Ben Langmead, Jeffrey T Leek
Nature Biotechnology (2017-04-11) https://doi.org/gf75hp
DOI: 10.1038/nbt.3838 · PMID: 28398307 · PMCID: PMC6742427

15. **Massive mining of publicly available RNA-seq data from human and mouse**
Alexander Lachmann, Denis Torre, Alexandra B. Keenan, Kathleen M. Jagodnik, Hoyjin J. Lee, Lily Wang, Moshe C. Silverstein, Avi Ma'ayan
Nature Communications (2018-04-10) https://doi.org/gc92dr
DOI: 10.1038/s41467-018-03751-6 · PMID: 29636450 · PMCID: PMC5893633

16. **Identification of therapeutic targets from genetic association studies using hierarchical component analysis**
Hao-Chih Lee, Osamu Ichikawa, Benjamin S. Glicksberg, Aparna A. Divaraniya, Christine E. Becker, Pankaj Agarwal, Joel T. Dudley
BioData Mining (2020-06-17) https://doi.org/gjp5pf
DOI: 10.1186/s13040-020-00216-9 · PMID: 32565911 · PMCID: PMC7301559

17. **Novel Variance-Component TWAS method for studying complex human diseases with applications to Alzheimer's dementia**
Shizhen Tang, Aron S. Buchman, Philip L. De Jager, David A. Bennett, Michael P. Epstein, Jingjing Yang
PLOS Genetics (2021-04-02) https://doi.org/gjpr3j
DOI: 10.1371/journal.pgen.1009482 · PMID: 33798195 · PMCID: PMC8046351

18. **Integrative approaches for large-scale transcriptome-wide association studies**
    Alexander Gusev, Arthur Ko, Huwenbo Shi, Gaurav Bhatia, Wonil Chung, Brenda WJH Penninx, Rick Jansen, Eco JC de Geus, Dorret I Boomsma, Fred A Wright, … Bogdan Pasaniuc
    Nature Genetics (2016-02-08) https://doi.org/f3vf4p
    DOI: 10.1038/ng.3506 · PMID: 26854917 · PMCID: PMC4767558

19. **Integrating predicted transcriptome from multiple tissues improves association detection**
    Alvaro N. Barbeira, Milton Pividori, Jiamao Zheng, Heather E. Wheeler, Dan L. Nicolae, Hae Kyung Im
    PLOS Genetics (2019-01-22) https://doi.org/ghs8vx
    DOI: 10.1371/journal.pgen.1007889 · PMID: 30668570 · PMCID: PMC6358100

20. **A gene-based association method for mapping traits using reference transcriptome data**
    Eric R Gamazon, Heather E Wheeler, Kaanan P Shah, Sahar V Mozaffari, Keston Aquino-Michaels, Robert J Carroll, Anne E Eyler, Joshua C Denny, Dan L Nicolae, Nancy J Cox, … GTEx Consortium
    Nature Genetics (2015-08-10) https://doi.org/f7p9zv
    DOI: 10.1038/ng.3367 · PMID: 26258848 · PMCID: PMC4552594

21. **Integrating Gene Expression with Summary Association Statistics to Identify Genes Associated with 30 Complex Traits**
    Nicholas Mancuso, Huwenbo Shi, Pagé Goddard, Gleb Kichaev, Alexander Gusev, Bogdan Pasaniuc
    The American Journal of Human Genetics (2017-03) https://doi.org/f9wvsg
    DOI: 10.1016/j.ajhg.2017.01.031 · PMID: 28238358 · PMCID: PMC5339290

22. **Heritability enrichment of specifically expressed genes identifies disease-relevant tissues and cell types**
    Hilary K. Finucane, Yakir A. Reshef, Verneri Anttila, Kamil Slowikowski, Alexander Gusev, Andrea Byrnes, Steven Gazal, Po-Ru Loh, Caleb Lareau, Noam Shoresh, … The Brainstorm Consortium
    Nature Genetics (2018-04-09) https://doi.org/gdfjqt
    DOI: 10.1038/s41588-018-0081-4 · PMID: 29632380 · PMCID: PMC5896795

23. **Integrating Autoimmune Risk Loci with Gene-Expression Data Identifies Specific Pathogenic Immune Cell Subsets**
    Xinli Hu, Hyun Kim, Eli Stahl, Robert Plenge, Mark Daly, Soumya Raychaudhuri
    The American Journal of Human Genetics (2011-10) https://doi.org/fpghp4
    DOI: 10.1016/j.ajhg.2011.09.002 · PMID: 21963258 · PMCID: PMC3188838

24. **SNPsea: an algorithm to identify cell types, tissues and pathways affected by risk loci**
    Kamil Slowikowski, Xinli Hu, Soumya Raychaudhuri
    Bioinformatics (2014-09-01) https://doi.org/f6j6v3
    DOI: 10.1093/bioinformatics/btu326 · PMID: 24813542 · PMCID: PMC4147889

25. **Meta-analysis of 375,000 individuals identifies 38 susceptibility loci for migraine**
    Padhraig Gormley, Verneri Anttila, Bendik S Winsvold, Priit Palta, Tonu Esko, Tune H Pers, Kai-How Farh, Ester Cuenca-Leon, Mikko Muona, Nicholas A Furlotte, … International Headache Genetics Consortium
    Nature Genetics (2016-06-20) https://doi.org/bmzx
    DOI: 10.1038/ng.3598 · PMID: 27322543 · PMCID: PMC5331903

26. **Biological interpretation of genome-wide association studies using predicted gene functions**
    Tune H. Pers, Juha M. Karjalainen, Yingleong Chan, Harm-Jan Westra, Andrew R. Wood, Jian Yang, Julian C. Lui, Sailaja Vedantam, Stefan Gustafsson, Tonu Esko, … Genetic Investigation of

ANthropometric Traits (GIANT) Consortium
Nature Communications (2015-01-19) https://doi.org/f3mwhd
DOI: 10.1038/ncomms6890 · PMID: 25597830 · PMCID: PMC4420238

27. **Estimating the causal tissues for complex traits and diseases**
Halit Ongen, Andrew A Brown, Olivier Delaneau, Nikolaos I Panousis, Alexandra C Nica, Emmanouil T Dermitzakis, GTEx Consortium
Nature Genetics (2017-10-23) https://doi.org/ggrr72
DOI: 10.1038/ng.3981 · PMID: 29058715

28. **A global overview of pleiotropy and genetic architecture in complex traits**
Kyoko Watanabe, Sven Stringer, Oleksandr Frei, Maša Umićević Mirkov, Christiaan de Leeuw, Tinca J. C. Polderman, Sophie van der Sluis, Ole A. Andreassen, Benjamin M. Neale, Danielle Posthuma
Nature Genetics (2019-08-19) https://doi.org/ggr84r
DOI: 10.1038/s41588-019-0481-0 · PMID: 31427789

29. **Detection and interpretation of shared genetic influences on 42 human traits**
Joseph K Pickrell, Tomaz Berisa, Jimmy Z Liu, Laure Ségurel, Joyce Y Tung, David A Hinds
Nature Genetics (2016-05-16) https://doi.org/f8ssw4
DOI: 10.1038/ng.3570 · PMID: 27182965 · PMCID: PMC5207801

30. **An Expanded View of Complex Traits: From Polygenic to Omnigenic**
Evan A. Boyle, Yang I. Li, Jonathan K. Pritchard
Cell (2017-06) https://doi.org/gcpgdz
DOI: 10.1016/j.cell.2017.05.038 · PMID: 28622505 · PMCID: PMC5536862

31. **Trans Effects on Gene Expression Can Drive Omnigenic Inheritance**
Xuanyao Liu, Yang I. Li, Jonathan K. Pritchard
Cell (2019-05) https://doi.org/gfz8bj
DOI: 10.1016/j.cell.2019.04.014 · PMID: 31051098 · PMCID: PMC6553491

32. **PhenomeXcan: Mapping the genome to the phenome through the transcriptome**
Milton Pividori, Padma S. Rajagopal, Alvaro Barbeira, Yanyu Liang, Owen Melia, Lisa Bastarache, YoSon Park, GTEx Consortium, Xiaoquan Wen, Hae K. Im
Science Advances (2020-09) https://doi.org/ghbvbf
DOI: 10.1126/sciadv.aba2083 · PMID: 32917697

33. **A Next Generation Connectivity Map: L1000 Platform and the First 1,000,000 Profiles**
Aravind Subramanian, Rajiv Narayan, Steven M. Corsello, David D. Peck, Ted E. Natoli, Xiaodong Lu, Joshua Gould, John F. Davis, Andrew A. Tubelli, Jacob K. Asiedu, … Todd R. Golub
Cell (2017-11) https://doi.org/cgwt
DOI: 10.1016/j.cell.2017.10.049 · PMID: 29195078 · PMCID: PMC5990023

34. **MultiPLIER: A Transfer Learning Framework for Transcriptomics Reveals Systemic Features of Rare Disease**
Jaclyn N. Taroni, Peter C. Grayson, Qiwen Hu, Sean Eddy, Matthias Kretzler, Peter A. Merkel, Casey S. Greene
Cell Systems (2019-05) https://doi.org/gf75g5
DOI: 10.1016/j.cels.2019.04.003 · PMID: 31121115 · PMCID: PMC6538307

35. **Pathway-level information extractor (PLIER) for gene expression data**
Weiguang Mao, Elena Zaslavsky, Boris M. Hartmann, Stuart C. Sealfon, Maria Chikina

Nature Methods (2019-06-27) https://doi.org/gf75g6

DOI: 10.1038/s41592-019-0456-1 · PMID: 31249421 · PMCID: PMC7262669

36. **The Electronic Medical Records and Genomics (eMERGE) Network: past, present, and future**
Omri Gottesman, Helena Kuivaniemi, Gerard Tromp, W. Andrew Faucett, Rongling Li, Teri A. Manolio, Saskia C. Sanderson, Joseph Kannry, Randi Zinberg, Melissa A. Basford, … and The eMERGE Network
Genetics in Medicine (2013-06-06) https://doi.org/f5dwbt

DOI: 10.1038/gim.2013.72 · PMID: 23743551 · PMCID: PMC3795928

37. **The UK Biobank resource with deep phenotyping and genomic data**
Clare Bycroft, Colin Freeman, Desislava Petkova, Gavin Band, Lloyd T. Elliott, Kevin Sharp, Allan Motyer, Damjan Vukcevic, Olivier Delaneau, Jared O'Connell, … Jonathan Marchini
Nature (2018-10-10) https://doi.org/gfb7h2

DOI: 10.1038/s41586-018-0579-z · PMID: 30305743 · PMCID: PMC6786975

38. **Finding function: evaluation methods for functional genomic data**
Chad L Myers, Daniel R Barrett, Matthew A Hibbs, Curtis Huttenhower, Olga G Troyanskaya
BMC Genomics (2006-07-25) https://doi.org/fg6wnk

DOI: 10.1186/1471-2164-7-187 · PMID: 16869964 · PMCID: PMC1560386

39. **The CAFA challenge reports improved protein function prediction and new functional annotations for hundreds of genes through experimental screens**
Naihui Zhou, Yuxiang Jiang, Timothy R. Bergquist, Alexandra J. Lee, Balint Z. Kacsoh, Alex W. Crocker, Kimberley A. Lewis, George Georghiou, Huy N. Nguyen, Md Nafiz Hamid, … Iddo Friedberg
Genome Biology (2019-11-19) https://doi.org/ggnxpz

DOI: 10.1186/s13059-019-1835-8 · PMID: 31744546 · PMCID: PMC6864930

40. **Estimating the population abundance of tissue-infiltrating immune and stromal cell populations using gene expression**
Etienne Becht, Nicolas A. Giraldo, Laetitia Lacroix, Bénédicte Buttard, Nabila Elarouci, Florent Petitprez, Janick Selves, Pierre Laurent-Puig, Catherine Sautès-Fridman, Wolf H. Fridman, Aurélien de Reyniès
Genome Biology (2016-10-20) https://doi.org/f87sgf

DOI: 10.1186/s13059-016-1070-5 · PMID: 27765066 · PMCID: PMC5073889

41. **MAGMA: Generalized Gene-Set Analysis of GWAS Data**
Christiaan A. de Leeuw, Joris M. Mooij, Tom Heskes, Danielle Posthuma
PLOS Computational Biology (2015-04-17) https://doi.org/gf92gp

DOI: 10.1371/journal.pcbi.1004219 · PMID: 25885710 · PMCID: PMC4401657

42. **Fast gene set enrichment analysis**
Gennady Korotkevich, Vladimir Sukhov, Nikolay Budin, Boris Shpak, Maxim N. Artyomov, Alexey Sergushichev
Cold Spring Harbor Laboratory (2021-02-01) https://doi.org/gfpqhm

DOI: 10.1101/060012

43. **DrugBank 4.0: shedding new light on drug metabolism**
Vivian Law, Craig Knox, Yannick Djoumbou, Tim Jewison, An Chi Guo, Yifeng Liu, Adam Maciejewski, David Arndt, Michael Wilson, Vanessa Neveu, … David S. Wishart
Nucleic Acids Research (2014-01) https://doi.org/f3mn6d

DOI: 10.1093/nar/gkt1068 · PMID: 24203711 · PMCID: PMC3965102

44. **Systematic integration of biomedical knowledge prioritizes drugs for repurposing**
Daniel Scott Himmelstein, Antoine Lizee, Christine Hessler, Leo Brueggeman, Sabrina L Chen, Dexter Hadley, Ari Green, Pouya Khankhanian, Sergio E Baranzini
eLife (2017-09-22) https://doi.org/cdfk
DOI: 10.7554/elife.26726 · PMID: 28936969 · PMCID: PMC5640425

45. **Dhimmel/Lincs V2.0: Refined Consensus Signatures From Lincs L1000**
Daniel Himmelstein, Leo Brueggeman, Sergio Baranzini
Zenodo (2016-03-08) https://doi.org/f3mqvr
DOI: 10.5281/zenodo.47223

46. **Computational Repositioning of the Anticonvulsant Topiramate for Inflammatory Bowel Disease**
J. T. Dudley, M. Sirota, M. Shenoy, R. K. Pai, S. Roedder, A. P. Chiang, A. A. Morgan, M. M. Sarwal, P. J. Pasricha, A. J. Butte
Science Translational Medicine (2011-08-17) https://doi.org/bmh5ts
DOI: 10.1126/scitranslmed.3002648 · PMID: 21849664 · PMCID: PMC3479650

47. **Discovery and Preclinical Validation of Drug Indications Using Compendia of Public Gene Expression Data**
M. Sirota, J. T. Dudley, J. Kim, A. P. Chiang, A. A. Morgan, A. Sweet-Cordero, J. Sage, A. J. Butte
Science Translational Medicine (2011-08-17) https://doi.org/c3fwxv
DOI: 10.1126/scitranslmed.3001318 · PMID: 21849665 · PMCID: PMC3502016

48. **Analysis of genome-wide association data highlights candidates for drug repositioning in psychiatry**
Hon-Cheong So, Carlos Kwan-Long Chau, Wan-To Chiu, Kin-Sang Ho, Cho-Pong Lo, Stephanie Ho-Yue Yim, Pak-Chung Sham
Nature Neuroscience (2017-08-14) https://doi.org/gbrssh
DOI: 10.1038/nn.4618 · PMID: 28805813

49. **Dhimmel/Indications V1.0. Pharmacotherapydb: The Open Catalog Of Drug Therapies For Disease**
Daniel S. Himmelstein, Pouya Khankhanian, Christine S. Hessler, Ari J. Green, Sergio E. Baranzini
Zenodo (2016-03-15) https://doi.org/f3mqwb
DOI: 10.5281/zenodo.47664

50. **Mechanism of Action of Niacin**
Vaijinath S. Kamanna, Moti L. Kashyap
The American Journal of Cardiology (2008-04) https://doi.org/c8zwdt
DOI: 10.1016/j.amjcard.2008.02.029 · PMID: 18375237

51. **Niacin: an old lipid drug in a new NAD+ dress**
Mario Romani, Dina Carina Hofer, Elena Katsyuba, Johan Auwerx
Journal of Lipid Research (2019-04) https://doi.org/gjpjft
DOI: 10.1194/jlr.s092007 · PMID: 30782960 · PMCID: PMC6446705

52. **The nicotinic acid receptor GPR109A (HM74A or PUMA-G) as a new therapeutic target**
S OFFERMANNS
Trends in Pharmacological Sciences (2006-07) https://doi.org/fgb4tr
DOI: 10.1016/j.tips.2006.05.008 · PMID: 16766048

53. **Langerhans Cells Release Prostaglandin D2 in Response to Nicotinic Acid**
Dominique Maciejewski-Lenoir, Jeremy G. Richman, Yaron Hakak, Ibragim Gaidarov, Dominic P. Behan, Daniel T. Connolly
Journal of Investigative Dermatology (2006-12) https://doi.org/dgxg75
DOI: 10.1038/sj.jid.5700586 · PMID: 17008871

54. **Nicotinic acid inhibits progression of atherosclerosis in mice through its receptor GPR109A expressed by immune cells**
Martina Lukasova, Camille Malaval, Andreas Gille, Jukka Kero, Stefan Offermanns
Journal of Clinical Investigation (2011-03-01) https://doi.org/cqftcq
DOI: 10.1172/jci41651 · PMID: 21317532 · PMCID: PMC3048854

55. **Role of HDL, ABCA1, and ABCG1 Transporters in Cholesterol Efflux and Immune Responses**
Laurent Yvan-Charvet, Nan Wang, Alan R. Tall
Arteriosclerosis, Thrombosis, and Vascular Biology (2010-02) https://doi.org/ds23w6
DOI: 10.1161/atvbaha.108.179283 · PMID: 19797709 · PMCID: PMC2812788

56. **Niacin Inhibits Apoptosis and Rescues Premature Ovarian Failure**
Shufang Wang, Min Sun, Ling Yu, Yixuan Wang, Yuanqing Yao, Deqing Wang
Cellular Physiology and Biochemistry (2018) https://doi.org/gfqvcq
DOI: 10.1159/000495051 · PMID: 30415247

57. **Chronic niacin administration ameliorates ovulation, histological changes in the ovary and adiponectin concentrations in a rat model of polycystic ovary syndrome**
Negin Asadi, Mahin Izadi, Ali Aflatounian, Mansour Esmaeili-Dehaj, Mohammad Ebrahim Rezvani, Zeinab Hafizi
Reproduction, Fertility and Development (2021) https://doi.org/gjpjkt
DOI: 10.1071/rd20306 · PMID: 33751926

58. **Clustering trees: a visualization for evaluating clusterings at multiple resolutions**
Luke Zappia, Alicia Oshlack
GigaScience (2018-07) https://doi.org/gfzqf5
DOI: 10.1093/gigascience/giy083 · PMID: 30010766 · PMCID: PMC6057528

59. **Prognostic value of grip strength: findings from the Prospective Urban Rural Epidemiology (PURE) study.**
Darryl P Leong, Koon K Teo, Sumathy Rangarajan, Patricio Lopez-Jaramillo, Alvaro Avezum, Andres Orlandini, Pamela Seron, Suad H Ahmed, Annika Rosengren, Roya Kelishadi, …
Lancet (London, England) (2015-05-13) https://www.ncbi.nlm.nih.gov/pubmed/25982160
DOI: 10.1016/s0140-6736(14)62000-6 · PMID: 25982160

60. **Densely Interconnected Transcriptional Circuits Control Cell States in Human Hematopoiesis**
Noa Novershtern, Aravind Subramanian, Lee N. Lawton, Raymond H. Mak, W. Nicholas Haining, Marie E. McConkey, Naomi Habib, Nir Yosef, Cindy Y. Chang, Tal Shay, … Benjamin L. Ebert
Cell (2011-01) https://doi.org/cf5k92
DOI: 10.1016/j.cell.2011.01.004 · PMID: 21241896 · PMCID: PMC3049864

61. **CD19 [+] CD5 [+] Cells as Indicators of Preeclampsia**
Federico Jensen, Gerd Wallukat, Florian Herse, Oliver Budner, Tarek El-Mousleh, Serban-Dan Costa, Ralf Dechend, Ana Claudia Zenclussen
Hypertension (2012-04) https://doi.org/gj36rs
DOI: 10.1161/hypertensionaha.111.188276 · PMID: 22353610

62. **Conditional and interaction gene-set analysis reveals novel functional pathways for blood pressure**
Christiaan A. de Leeuw, Sven Stringer, Ilona A. Dekkers, Tom Heskes, Danielle Posthuma
Nature Communications (2018-09-14) https://doi.org/gd6d85
DOI: 10.1038/s41467-018-06022-6 · PMID: 30218068 · PMCID: PMC6138636

63. **Estrogen and hypertension**
Muhammad S. Ashraf, Wanpen Vongpatanasin
Current Hypertension Reports (2006-09) https://doi.org/d638rf
DOI: 10.1007/s11906-006-0080-1 · PMID: 16965722

64. **Depression as a predictor for coronary heart disease. a review and meta-analysis.**
Reiner Rugulies
American journal of preventive medicine (2002-07)
https://www.ncbi.nlm.nih.gov/pubmed/12093424
DOI: 10.1016/s0749-3797(02)00439-7 · PMID: 12093424

65. **Mental Disorders Across the Adult Life Course and Future Coronary Heart Disease**
Catharine R. Gale, G. David Batty, David P. J. Osborn, Per Tynelius, Finn Rasmussen
Circulation (2014-01-14) https://doi.org/qm4
DOI: 10.1161/circulationaha.113.002065 · PMID: 24190959 · PMCID: PMC4107269

66. **Mortality gap for people with bipolar disorder and schizophrenia: UK-based cohort study 2000–2014**
Joseph F. Hayes, Louise Marston, Kate Walters, Michael B. King, David P. J. Osborn
British Journal of Psychiatry (2018-01-02) https://doi.org/gbwcjx
DOI: 10.1192/bjp.bp.117.202606 · PMID: 28684403 · PMCID: PMC5579328

67. **Getting to the Heart of Alzheimer Disease**
Joshua M. Tublin, Jeremy M. Adelstein, Federica del Monte, Colin K. Combs, Loren E. Wold
Circulation Research (2019-01-04) https://doi.org/gjzjgq
DOI: 10.1161/circresaha.118.313563 · PMID: 30605407 · PMCID: PMC6319653

68. **The overlap between vascular disease and Alzheimer's disease - lessons from pathology**
Johannes Attems, Kurt A Jellinger
BMC Medicine (2014-11-11) https://doi.org/f6pjd4
DOI: 10.1186/s12916-014-0206-2 · PMID: 25385447 · PMCID: PMC4226890

69. **Cardiovascular Risk Factors for Alzheimer's Disease**
Clive Rosendorff, Michal S. Beeri, Jeremy M. Silverman
The American Journal of Geriatric Cardiology (2007-03) https://doi.org/bpfw5d
DOI: 10.1111/j.1076-7460.2007.06696.x · PMID: 17483665

70. **Reverse cholesterol transport and cholesterol efflux in atherosclerosis**
R. Ohashi, H. Mu, X. Wang, Q. Yao, C. Chen
QJM: An International Journal of Medicine (2005-12) https://doi.org/dn2fgt
DOI: 10.1093/qjmed/hci136 · PMID: 16258026

71. **recount3: summaries and queries for large-scale RNA-seq expression and splicing**
Christopher Wilks, Shijie C. Zheng, Feng Yong Chen, Rone Charles, Brad Solomon, Jonathan P. Ling, Eddie Luidy Imada, David Zhang, Lance Joseph, Jeffrey T. Leek, … Ben Langmead
Cold Spring Harbor Laboratory (2021-05-25) https://doi.org/gj7cmq
DOI: 10.1101/2021.05.21.445138

72. **Opportunities and challenges for transcriptome-wide association studies**

Michael Wainberg, Nasa Sinnott-Armstrong, Nicholas Mancuso, Alvaro N. Barbeira, David A. Knowles, David Golan, Raili Ermel, Arno Ruusalepp, Thomas Quertermous, Ke Hao, … Anshul Kundaje

Nature Genetics (2019-03-29) https://doi.org/gf3hmr

DOI: 10.1038/s41588-019-0385-z · PMID: 30926968 · PMCID: PMC6777347

73. **Probabilistic colocalization of genetic variants from complex and molecular traits: promise and limitations**

Abhay Hukku, Milton Pividori, Francesca Luca, Roger Pique-Regi, Hae Kyung Im, Xiaoquan Wen

The American Journal of Human Genetics (2021-01) https://doi.org/gj58gg

DOI: 10.1016/j.ajhg.2020.11.012 · PMID: 33308443 · PMCID: PMC7820626

74. **Transcriptome-wide association study of schizophrenia and chromatin activity yields mechanistic disease insights**

Alexander Gusev, Nicholas Mancuso, Hyejung Won, Maria Kousi, Hilary K. Finucane, Yakir Reshef, Lingyun Song, Alexias Safi, Steven McCarroll, Benjamin M. Neale, … Schizophrenia Working Group of the Psychiatric Genomics Consortium

Nature Genetics (2018-04-09) https://doi.org/gdfdf2

DOI: 10.1038/s41588-018-0092-1 · PMID: 29632383 · PMCID: PMC5942893

75. **Shared genetic origin of asthma, hay fever and eczema elucidates allergic disease biology**

Manuel A Ferreira, Judith M Vonk, Hansjörg Baurecht, Ingo Marenholz, Chao Tian, Joshua D Hoffman, Quinta Helmer, Annika Tillander, Vilhelmina Ullemar, Jenny van Dongen, … LifeLines Cohort Study

Nature Genetics (2017-10-30) https://doi.org/gchg62

DOI: 10.1038/ng.3985 · PMID: 29083406 · PMCID: PMC5989923

76. **A genome-wide cross-trait analysis from UK Biobank highlights the shared genetic architecture of asthma and allergic diseases**

Zhaozhong Zhu, Phil H. Lee, Mark D. Chaffin, Wonil Chung, Po-Ru Loh, Quan Lu, David C. Christiani, Liming Liang

Nature Genetics (2018-05-21) https://doi.org/gdpmtn

DOI: 10.1038/s41588-018-0121-0 · PMID: 29785011 · PMCID: PMC5980765

77. **Systematic tissue annotations of –omics samples by modeling unstructured metadata**

Nathaniel T. Hawkins, Marc Maldaver, Anna Yannakopoulos, Lindsay A. Guare, Arjun Krishnan

Cold Spring Harbor Laboratory (2021-05-20) https://doi.org/gj2pkc

DOI: 10.1101/2021.05.10.443525

78. **Exploring the phenotypic consequences of tissue specific gene expression variation inferred from GWAS summary statistics**

Alvaro N. Barbeira, Scott P. Dickinson, Rodrigo Bonazzola, Jiamao Zheng, Heather E. Wheeler, Jason M. Torres, Eric S. Torstenson, Kaanan P. Shah, Tzintzuni Garcia, Todd L. Edwards, … GTEx Consortium

Nature Communications (2018-05-08) https://doi.org/gdjvp5

DOI: 10.1038/s41467-018-03621-1 · PMID: 29739930 · PMCID: PMC5940825

79. **Probabilistic Colocalization of Genetic Variants from Complex and Molecular Traits: Promise and Limitations**

Abhay Hukku, Milton Pividori, Francesca Luca, Roger Pique-Regi, Hae Kyung Im, Xiaoquan Wen

Cold Spring Harbor Laboratory (2020-07-01) https://doi.org/gjwh3p

DOI: 10.1101/2020.07.01.182097

80. **The Molecular Signatures Database Hallmark Gene Set Collection**
Arthur Liberzon, Chet Birger, Helga Thorvaldsdóttir, Mahmoud Ghandi, Jill P. Mesirov, Pablo Tamayo
Cell Systems (2015-12) https://doi.org/gf78hq
DOI: 10.1016/j.cels.2015.12.004 · PMID: 26771021 · PMCID: PMC4707969

81. **A global reference for human genetic variation**
The 1000 Genomes Project Consortium
Nature (2015-09-30) https://doi.org/73d
DOI: 10.1038/nature15393 · PMID: 26432245 · PMCID: PMC4750478

82. **GWAS summary statistics imputation support data and integration with PrediXcan MASHR**
Alvaro Numa Barbeira, Hae Kyung Im
Zenodo (2019-12-10) https://doi.org/gj6jwq
DOI: 10.5281/zenodo.3657902

83. **Human Disease Ontology 2018 update: classification, content and workflow expansion**
Lynn M Schriml, Elvira Mitraka, James Munro, Becky Tauber, Mike Schor, Lance Nickle, Victor Felix, Linda Jeng, Cynthia Bearer, Richard Lichenstein, … Carol Greene
Nucleic Acids Research (2019-01-08) https://doi.org/ggx9wp
DOI: 10.1093/nar/gky1032 · PMID: 30407550 · PMCID: PMC6323977

84. **Modeling sample variables with an Experimental Factor Ontology**
James Malone, Ele Holloway, Tomasz Adamusiak, Misha Kapushesky, Jie Zheng, Nikolay Kolesnikov, Anna Zhukova, Alvis Brazma, Helen Parkinson
Bioinformatics (2010-04-15) https://doi.org/dsb6vt
DOI: 10.1093/bioinformatics/btq099 · PMID: 20200009 · PMCID: PMC2853691

85. **EBISPOT/EFO-UKB-mappings**
EBISPOT
(2021-03-15) https://github.com/EBISPOT/EFO-UKB-mappings

86. **Comparing partitions**
Lawrence Hubert, Phipps Arabie
Journal of Classification (1985-12) https://doi.org/bphmzh
DOI: 10.1007/bf01908075

87. **Combining multiple clusterings using evidence accumulation**
Ana L. N. Fred, Anil K. Jain
IEEE Transactions on Pattern Analysis and Machine Intelligence (2005-06) https://doi.org/bsknv6
DOI: 10.1109/tpami.2005.113 · PMID: 15943417

88. **Diversity control for improving the analysis of consensus clustering**
Milton Pividori, Georgina Stegmayer, Diego H. Milone
Information Sciences (2016-09) https://doi.org/ghtqbk
DOI: 10.1016/j.ins.2016.04.027

89. **A Link-Based Approach to the Cluster Ensemble Problem**
Natthakan Iam-On, Tossapon Boongoen, Simon Garrett, Chris Price
IEEE Transactions on Pattern Analysis and Machine Intelligence (2011-12) https://doi.org/cqgkh3
DOI: 10.1109/tpami.2011.84 · PMID: 21576752

90. **Hybrid clustering solution selection strategy**
Zhiwen Yu, Le Li, Yunjun Gao, Jane You, Jiming Liu, Hau-San Wong, Guoqiang Han
Pattern Recognition (2014-10) https://doi.org/ghtzwt
DOI: 10.1016/j.patcog.2014.04.005

91. **UMAP: Uniform Manifold Approximation and Projection for Dimension Reduction**
Leland McInnes, John Healy, James Melville
arXiv (2020-09-21) https://arxiv.org/abs/1802.03426

92. **k-means++: the advantages of careful seeding**
David Arthur, Sergei Vassilvitskii
Proceedings of the Eighteenth Annual ACM-SIAM Symposium on Discrete Algorithms (2007)
http://ilpubs.stanford.edu:8090/778/1/2006-13.pdf

93. **On Spectral Clustering: Analysis and an algorithm**
Andrew Ng, Michael Jordan, Yair Weiss
Advances in Neural Information Processing Systems (2001)
https://ai.stanford.edu/~ang/papers/nips01-spectral.pdf

94. **A Density-Based Algorithm for Discovering Clusters in Large Spatial Databases with Noise**
Martin Ester, Hans-Peter Kriegel, Jörg Sander, Xiaowei Xu
Proceedings of the Second International Conference on Knowledge Discovery and Data Mining (1996) https://www.aaai.org/Papers/KDD/1996/KDD96-037.pdf

95. **Optimized sgRNA design to maximize activity and minimize off-target effects of CRISPR-Cas9.**
John G Doench, Nicolo Fusi, Meagan Sullender, Mudra Hegde, Emma W Vaimberg, Katherine F Donovan, Ian Smith, Zuzana Tothova, Craig Wilen, Robert Orchard, … David E Root
Nature biotechnology (2016-01-18) https://www.ncbi.nlm.nih.gov/pubmed/26780180
DOI: 10.1038/nbt.3437 · PMID: 26780180 · PMCID: PMC4744125

96. **Homo sapiens (ID 232177) - BioProject - NCBI**
https://www.ncbi.nlm.nih.gov/bioproject/PRJNA232177

Supplementary material

CRISPR-screen
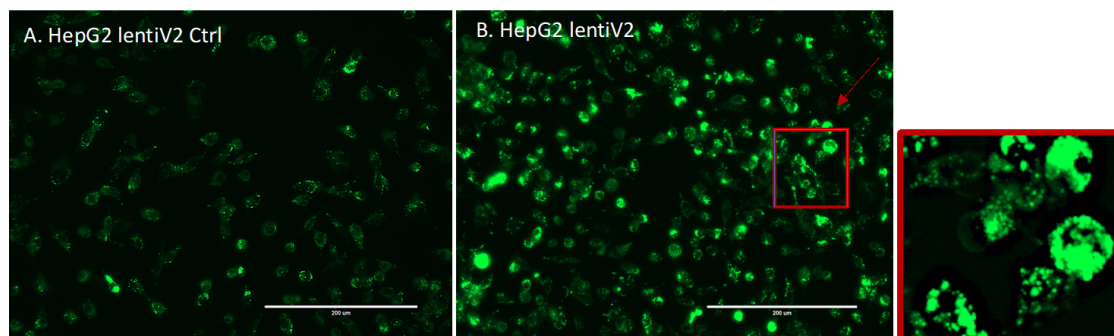
Figure 7: EVOS Fluorescent Microscope Image Capture. A. HepG2_lentiV2_Ctrl with no-viral transduction. B. HepG2_lentiV2 with viral transduction.
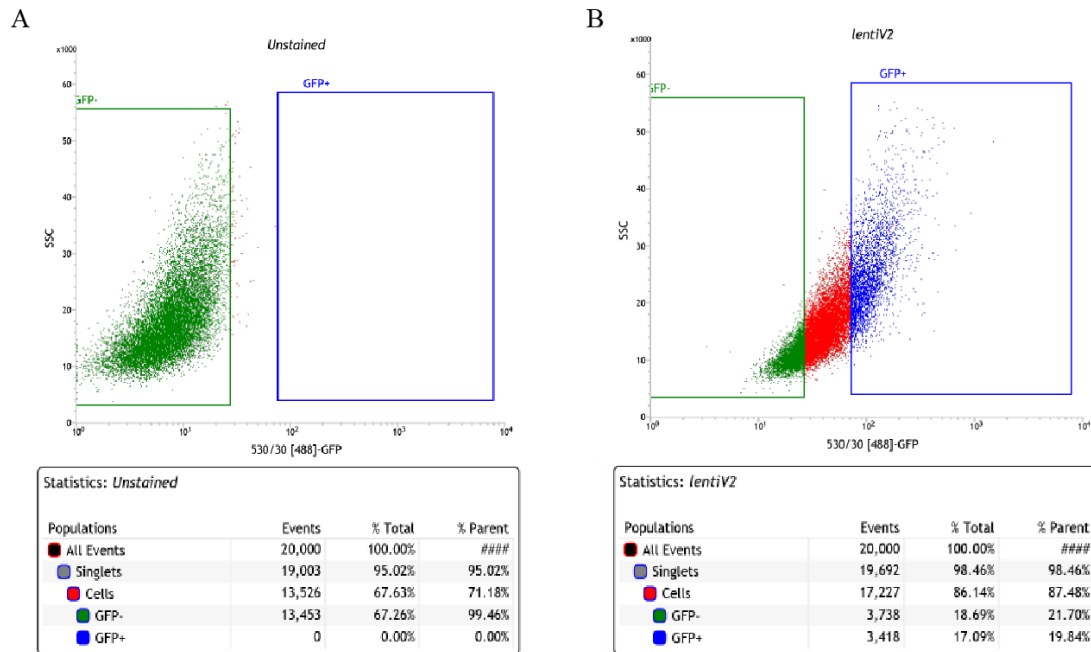
Figure 8: Fluorescence-Activated Cell Sorting Gate Setting. A. HepG2_UnStained WT. B. HepG2_lentiV2 with viral transduction.
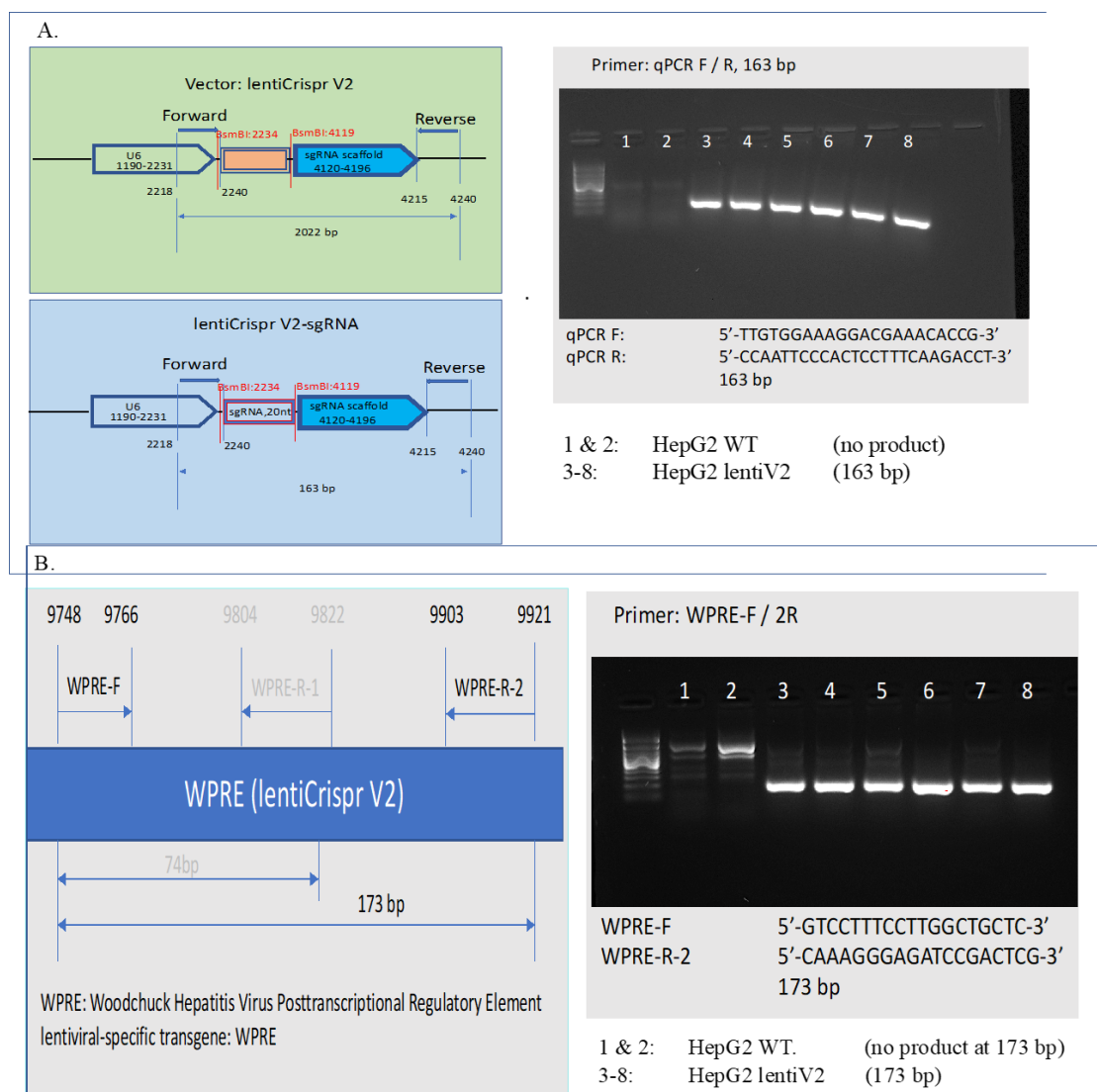
Figure 9: Verification of sgRNA cassette and lentiV2 transgene. A. 20nt sgRNA cassette was verified in lentiV2 transduced genomic DNA population, 163 bp PCR product obtained, while WT HepG2 didn't possess the cassette, thus, no PCR product. B. lentiviral-specific transgene WPRE was verified in lentiV2 transduced genomic DNA population, while no transduced WT didn't have the transgene, therefore, no 173 bp PCR product observed.

Table 1. Primers for Generating Illumina Libraries

P5/P7 flowcell attachment sequence
Illumina sequencing primer
Vector primer binding sequence
Stagger region / Barcode region

P5 primer :
5'AATGATACGGCGACCACCGAGATCTACACTCTTTCCCTACACGACGCTCTTCCGATCT[s]TTGTGGAAAGGACGAAACACCG

P7 primer:
5'CAAGCAGAAGACGGCATACGAGATNNNNNNNNGTGACTGGAGTTCAGACGTGTGCTCTTCCGATCTCCAATTCCCACTCCTTTCAAGACCT

P5 Stagger Region sequences ([s])		P7 barcode (index) sequences (NNNNNNNN)	
	Stagger Sequence to include in P5 primer, 5'-3'		Sequence to include in P7 primer, 5'-3'
P5 0 nt		P7-001	CGGTTCAA
P5 1nt	C	P7-002	GCTGGATT
P5 2 nt	GC	P7-003	TAACTCGG
P5 3 nt	AGC	P7-004	TAACAGTT
P5 4 nt	CAAC	P7-005	ATACTCAA
P5 6 nt	TGCACC	P7-006	GCTGAGAA
P5 7nt	ACGCAAC	P7-007	ATTGGAGG
P5 8nt	GAAGACCC	P7-008	TAGTCTAA
		P7-009	CGGTGACC

Figure 10:

A. Construct For Illumina Library Generation
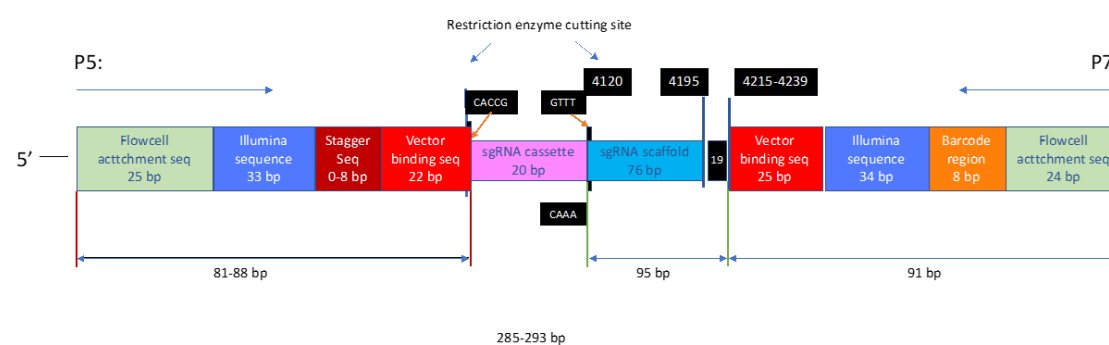
B. 2100 expert_High Sensitivity DNA Assay
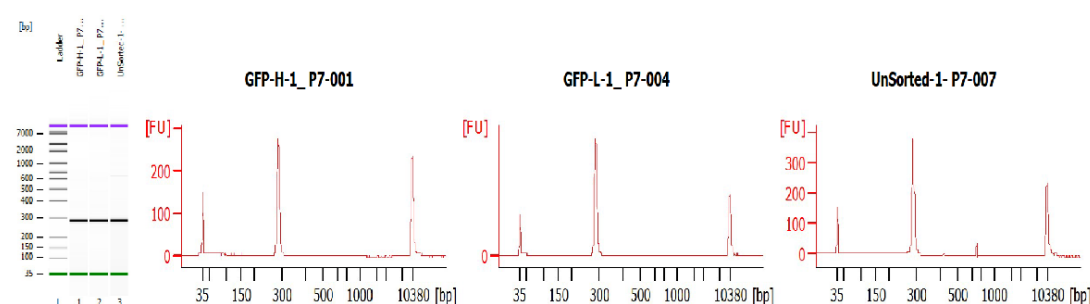
Figure 11: Illumina library generation. A. Construct for generating illumina libraries. B. Final illumina library from HS DNA —showed a single ~285bp peak was generated.

Gene modules enriched for lipids gene-sets

Table 1: Gene modules (LVs) enriched for lipids gene-sets found with CRISPR screening.

Gene module	Lipids gene-set	p-value	FDR
LV678	decrease	2.61e-07	2.57e-04
LV707	increase	1.74e-07	2.57e-04
LV905	increase	4.29e-05	2.82e-02
LV915	increase	6.37e-05	3.14e-02

Top traits across lipids-associated genes and modules

Table 2: Top 25 traits associated with genes from the lipids-decreasing gene-set found with CRISPR screening.

Order	Trait	Category
1	Vascular/heart problems diagnosed by doctor: High blood pressure	Diseases (cardiovascular)
2	Diastolic blood pressure, automated reading	Blood pressure
3	Non-cancer illness code, self-reported: hypertension	Diseases (cardiovascular)
4	Suggestive for eosinophilic asthma	Diseases (FinnGen)
5	Medication for cholesterol, blood pressure, diabetes, or take exogenous hormones: Blood pressure medication	Medication
6	Forced expiratory volume in 1-second (FEV1), predicted	Spirometry
7	Vascular/heart problems diagnosed by doctor: None of the above	Diseases (cardiovascular)
8	Treatment/medication code: levothyroxine sodium	Medications
9	Haematocrit percentage	Blood count
10	Treatment/medication code: lisinopril	Medications
11	Haemoglobin concentration	Blood count
12	Job coding: counter clerk, bank clerk, cashier, post office clerk	Employment history
13	Acute alcohol intoxication	Diseases (FinnGen)
14	Systolic blood pressure, automated reading	Blood pressure
15	Platelet count	Blood count
16	Red Blood Cell Count	Blood
17	Peak expiratory flow (PEF)	Spirometry
18	Sitting height	Body size measures
19	Treatment/medication code: bendroflumethiazide	Medications
20	Age started wearing glasses or contact lenses	Eyesight
21	Comparative height size at age 10	Early life factors
22	Workplace very cold: Often	Employment history
23	Salt added to food	Diet
24	Difficulty concentrating during worst period of anxiety	Anxiety
25	Treatment/medication code: metformin	Medications

Table 3: Top 25 traits associated with gene modules (LVs) enriched for the lipids-decreasing gene-set found with CRISPR screening.

Order	Trait	Category
1	Non-cancer illness code, self-reported: malabsorption/coeliac disease	Diseases (gastrointestinal/abdominal)

Order	Trait	Category
2	Diastolic blood pressure, automated reading	Blood pressure
3	Immature reticulocyte fraction	Blood count
4	Treatment/medication code: ferrous salt product	Medications
5	Vascular/heart problems diagnosed by doctor: None of the above	Diseases (cardiovascular)
6	Platelet distribution width	Blood count
7	Unstable angina pectoris	Diseases (FinnGen)
8	Vascular/heart problems diagnosed by doctor: High blood pressure	Diseases (cardiovascular)
9	Nucleated red blood cell count	Blood count
10	Diagnoses - main ICD10: K90 Intestinal malabsorption	Diseases (ICD10 main)
11	Coeliac disease	Diseases (FinnGen)
12	Non-cancer illness code, self-reported: hypertension	Diseases (cardiovascular)
13	Nucleated red blood cell percentage	Blood count
14	Relative age of first facial hair	Male-specific factors
15	Treatment/medication code: thiamine preparation	Medications
16	Diagnoses - main ICD10: I70 Atherosclerosis	Diseases (ICD10 main)
17	White Blood Cell Count	Blood
18	Treatment/medication code: gtn 400micrograms spray	Medications
19	Treatment/medication code: singulair 10mg tablet	Medications
20	Difficulty not smoking for 1 day	Smoking
21	Mean reticulocyte volume	Blood count
22	Other malignant neoplasms of skin	Diseases (FinnGen)
23	Length of working week for main job	Employment
24	Pulse rate, automated reading	Blood pressure
25	Milk type used: Skimmed	Diet

Table 4: Top 25 traits associated with genes from the lipids-increasing gene-set found with CRISPR screening.

Order	Trait	Category
1	Lymphocyte percentage	Blood count
2	Neutrophill percentage	Blood count
3	Neutrophill count	Blood count
4	Red blood cell (erythrocyte) count	Blood count
5	Lymphocyte Count	Blood
6	Trunk predicted mass	Impedance measures
7	Trunk fat-free mass	Impedance measures
8	Mean corpuscular volume	Blood count
9	Mean sphered cell volume	Blood count
10	White blood cell (leukocyte) count	Blood count

Order	Trait	Category
11	Skin colour	Sun exposure
12	Arm fat-free mass (left)	Impedance measures
13	Impedance of arm (left)	Impedance measures
14	Mean reticulocyte volume	Blood count
15	Whole body water mass	Impedance measures
16	Impedance of arm (right)	Impedance measures
17	Mean corpuscular haemoglobin	Blood count
18	Whole body fat-free mass	Impedance measures
19	Arm predicted mass (left)	Impedance measures
20	Arm predicted mass (right)	Impedance measures
21	Arm fat-free mass (right)	Impedance measures
22	Hair colour (natural, before greying): Red	Sun exposure
23	Ease of skin tanning	Sun exposure
24	High light scatter reticulocyte count	Blood count
25	White Blood Cell Count	Blood

Table 5: Top 25 traits associated with gene modules (LVs) enriched for the lipids-increasing gene-set found with CRISPR screening.

Order	Trait	Category
1	Ankle spacing width	Bone-densitometry of heel
2	Ankle spacing width (left)	Bone-densitometry of heel
3	Ankle spacing width (right)	Bone-densitometry of heel
4	Job SOC coding: Advertising and public relations managers	Employment history
5	Hair colour (natural, before greying): Red	Sun exposure
6	Sitting height	Body size measures
7	Platelet distribution width	Blood count
8	Non-cancer illness code, self-reported: malabsorption/coeliac disease	Diseases (gastrointestinal/abdominal)
9	Job coding: advertising or public relations manager, media/publicity manager, campaign/fundraising manager	Employment history
10	Forced expiratory volume in 1-second (FEV1), predicted	Spirometry
11	Heel Broadband ultrasound attenuation, direct entry	Bone-densitometry of heel
12	Intra-ocular pressure, Goldmann-correlated (right)	Intraocular pressure
13	Hearing test done: No, I am unable to do this	Hearing test
14	Rheumatoid Arthritis	Diseases (ICD10 main)
15	Red blood cell (erythrocyte) distribution width	Blood count
16	Job coding: childminder, au pair, children's nanny	Employment history

Order	Trait	Category
17	Heel bone mineral density (BMD)	Bone-densitometry of heel
18	Heel quantitative ultrasound index (QUI), direct entry	Bone-densitometry of heel
19	Heel bone mineral density (BMD) T-score, automated	Bone-densitometry of heel
20	Job SOC coding: Hand craft occupations n.e.c.	Employment history
21	Reason for glasses/contact lenses: For just reading/near work as you are getting older (called 'presbyopia')	Eyesight
22	Intra-ocular pressure, Goldmann-correlated (left)	Intraocular pressure
23	Pulse wave peak to peak time	Arterial stiffness
24	Hand grip strength (left)	Hand grip strength
25	Treatment/medication code: luteine	Medications

LV246
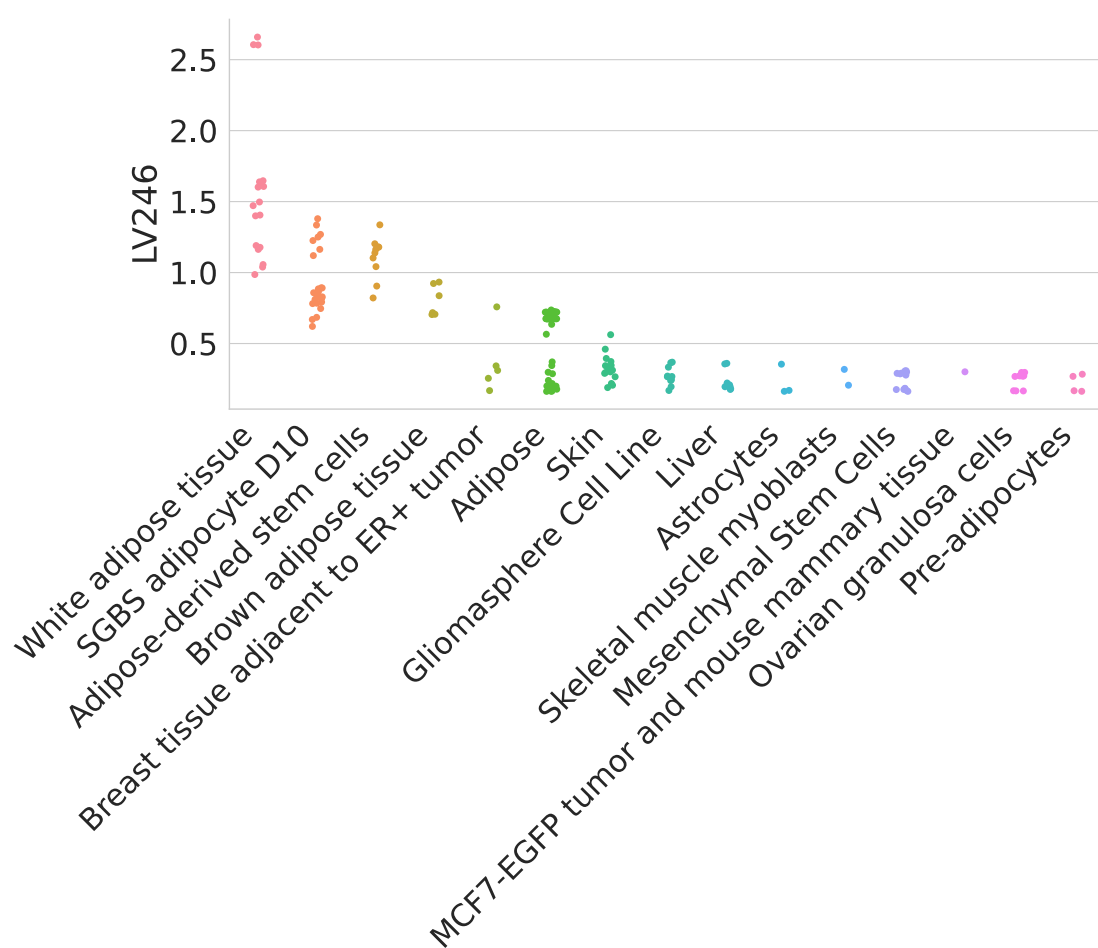
Figure 12: Cell types for LV246.

Table 6: Pathways aligned to LV246.

Pathway	AUC	p-value (adjusted)
REACTOME_FATTY_ACID_TRIACYLGLYCEROL_AND_KETONE_BODY_METABOLISM	0.89	3.97e-16
REACTOME_METABOLISM_OF_LIPIDS_AND_LIPOPROTEINS	0.67	1.14e-08

Pathway	AUC	p-value (adjusted)
REACTOME_TRIGLYCERIDE_BIOSYNTHESIS	0.86	6.52e-04
KEGG_PYRUVATE_METABOLISM	0.82	2.66e-03
KEGG_PROPANOATE_METABOLISM	0.83	4.27e-03

Table 7: Significant trait associations of LV246 in PhenomeXcan.

Trait description	Sample size	Cases	Partition/cluster number	p-value (adjusted)
CH2DB NMR	24,154		29 / 16	9.36e-11
Non-cancer illness code, self-reported: high cholesterol	361,141	43,957	29 / 17	5.24e-05
Medication for cholesterol, blood pressure, diabetes, or take exogenous hormones: Cholesterol lowering medication	193,148	24,247	29 / 17	9.34e-03
HDL Cholesterol NMR	19,270		29 / 16	9.34e-03
Fasting Glucose	46,186		29 / 11	4.13e-02

Table 8: Significant trait associations of LV246 in eMERGE.

Phecode	Trait description	Sample size	Cases	p-value (adjusted)

LV678
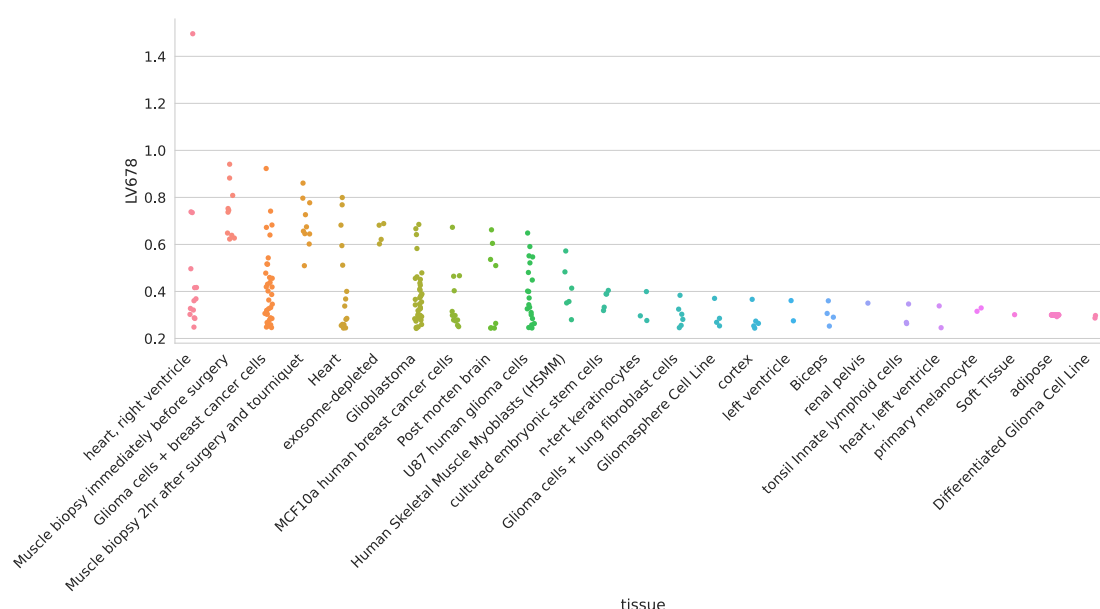
Figure 13: Cell types for LV678.

Table 9: Pathways aligned to LV678.

Pathway	AUC	p-value (adjusted)

Pathway	AUC	p-value (adjusted)
KEGG_OXIDATIVE_PHOSPHORYLATION	0.98	5.75e-14
REACTOME_RESPIRATORY_ELECTRON_TRANSPORT_ATP_SYNTHESIS_BY_CHEMIOSMOTIC_COUPLING_AND_HEAT_PRODUCTION_BY_UNCOUPLING_PROTEINS_	0.99	5.94e-11
REACTOME_RESPIRATORY_ELECTRON_TRANSPORT	1.00	3.10e-09
REACTOME_TCA_CYCLE_AND_RESPIRATORY_ELECTRON_TRANSPORT	0.86	9.66e-09
MIPS_55S_RIBOSOME_MITOCHONDRIAL	0.81	8.20e-05
REACTOME_SRP_DEPENDENT_COTRANSLATIONAL_PROTEIN_TARGETING_TO_MEMBRANE	0.69	6.03e-03
REACTOME_MITOCHONDRIAL_PROTEIN_IMPORT	0.74	1.99e-02

Table 10: Significant trait associations of LV678 in PhenomeXcan.

Trait description	Sample size	Cases	Partition/cluster number	p-value (adjusted)
Vascular/heart problems diagnosed by doctor: Heart attack	360,420	8,288	29 / 14	1.08e-02
Inflammatory Bowel Disease	34,652	12,882	29 / 21	2.35e-02
Non-cancer illness code, self-reported: heart attack/myocardial infarction	361,141	8,239	29 / 14	2.35e-02

Table 11: Significant trait associations of LV678 in eMERGE.

Phecode	Trait description	Sample size	Cases	p-value (adjusted)

LV116
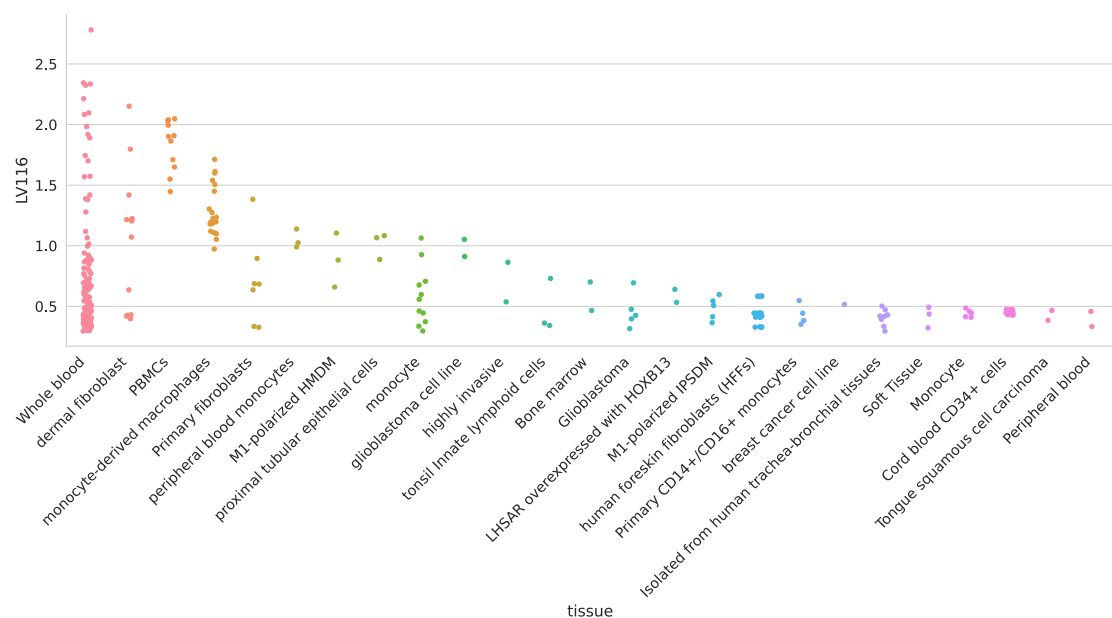
Figure 14: Cell types for LV116.

LV931
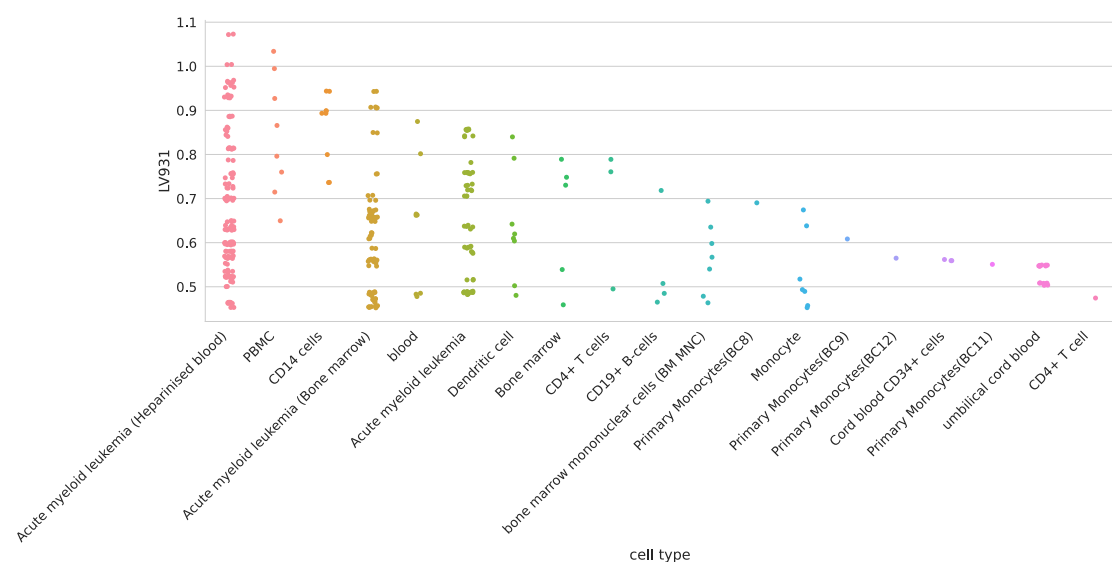
Figure 15: Cell types for LV931.

LV66
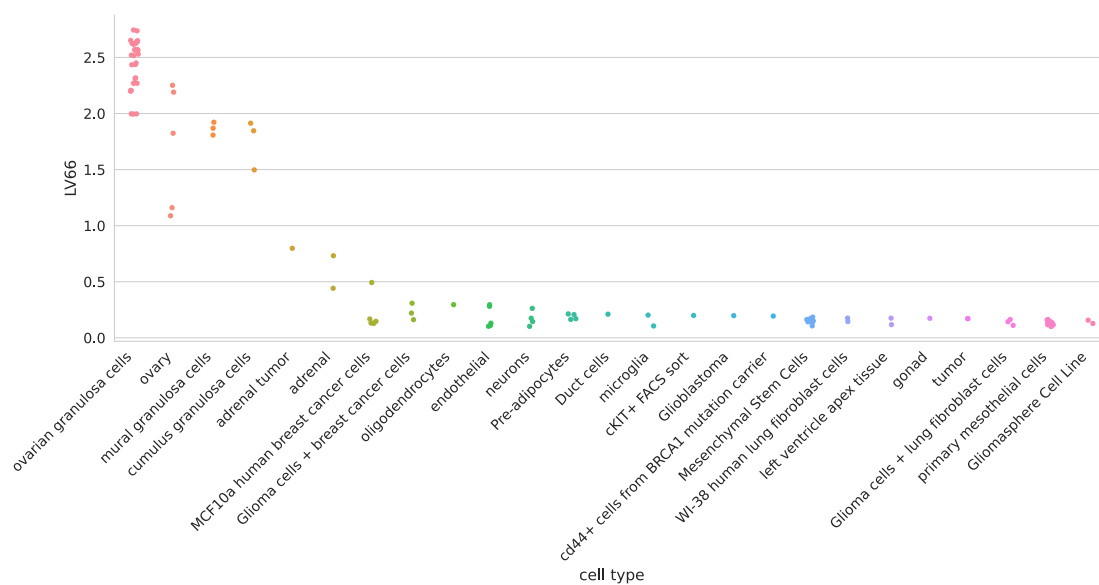
Figure 16: Cell types for LV66.

LV928
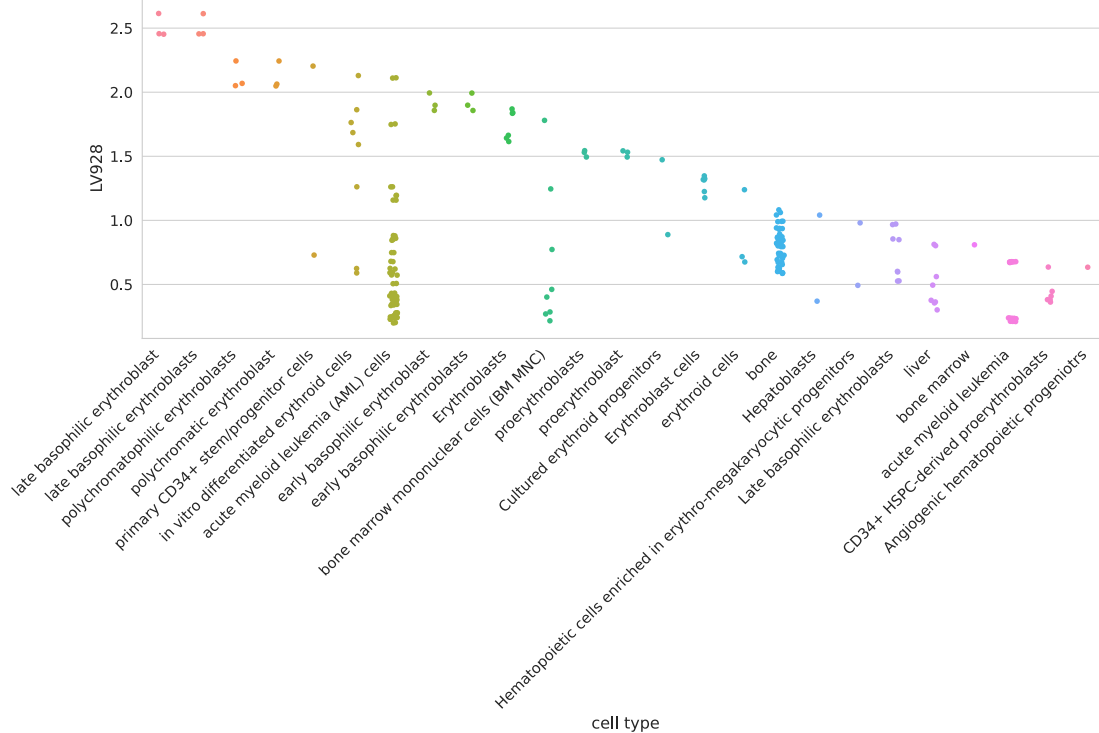
Figure 17: Cell types for LV928.

LV30
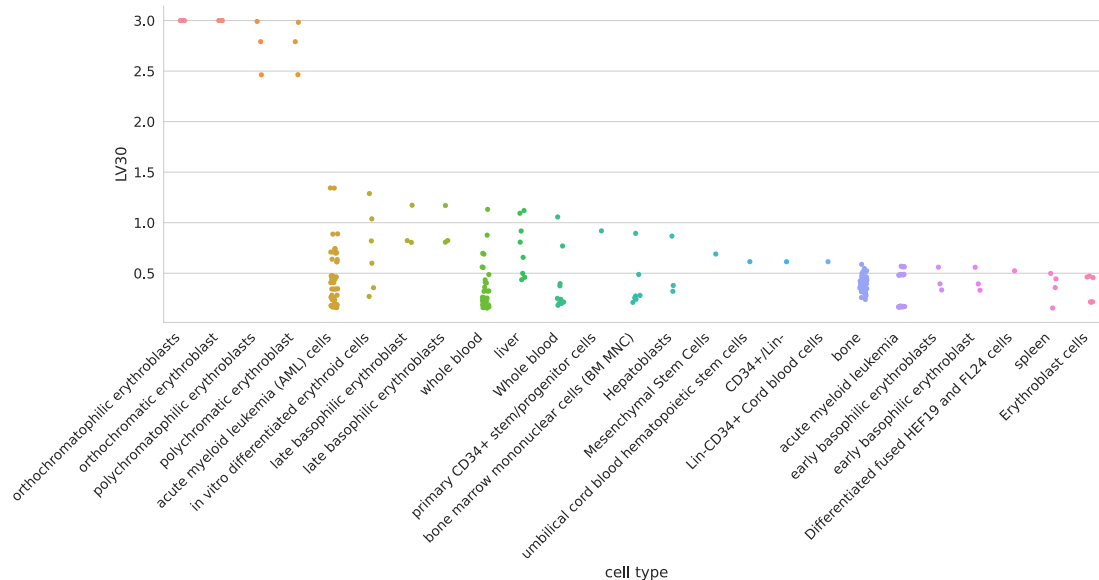
Figure 18: Cell types for LV30.

LV730
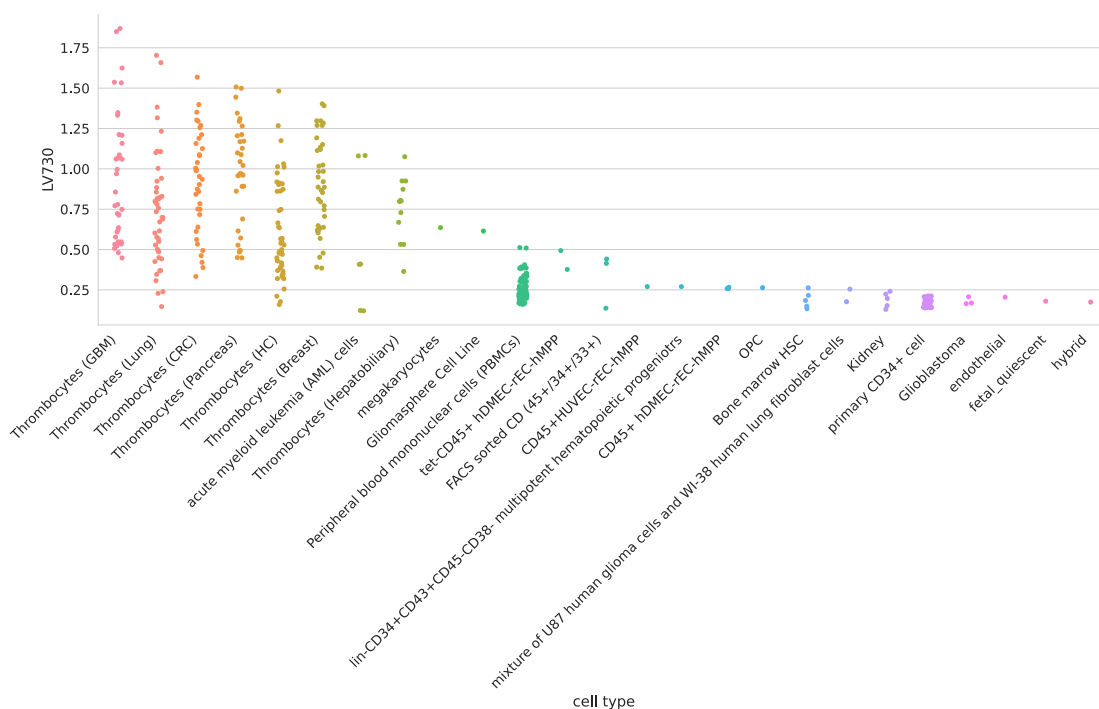
Figure 19: Cell types for LV730.

LV598

Figure 20: Cell types for LV598.

Table 12: Significant trait associations of LV598 in PhenomeXcan.

Trait description	Sample size	Cases	Partition/cluster number	p-value (adjusted)
6mm strong meridian (right)	66,256		29 / 10	4.13e-07
6mm weak meridian (right)	66,256		29 / 10	2.63e-06
6mm strong meridian (left)	65,551		29 / 10	3.13e-06
3mm strong meridian (left)	75,398		29 / 10	3.24e-06
6mm weak meridian (left)	65,551		29 / 10	1.53e-05
3mm weak meridian (left)	75,398		29 / 10	2.00e-05
3mm strong meridian (right)	75,410		29 / 10	3.70e-05
3mm weak meridian (right)	75,410		29 / 10	4.81e-05

LV155

Figure 21: Cell types for LV155.

Table 13: Significant trait associations of LV155 in PhenomeXcan.

Trait description	Sample size	Cases	Partition/cluster number	p-value (adjusted)
Non-cancer illness code, self-reported: hypothyroidism/myxoedema	361,141	17,574	29 / 13	2.01e-03
Non-cancer illness code, self-reported: hyperthyroidism/thyrotoxicosis	361,141	2,730	29 / 13	1.29e-02
Treatment/medication code: levothyroxine sodium	361,141	14,689	29 / 13	1.41e-02

Table 14: Significant trait associations of LV155 in eMERGE.

Phecode	Trait description	Sample size	Cases	p-value (adjusted)
244.2	Acquired hypothyroidism	45,839	1,155	2.19e-02
427.9	Palpitations	35,214	6,092	4.43e-02

LV844

Figure 22: Cell types for LV844.

Table 15: Significant trait associations of LV844 in PhenomeXcan.

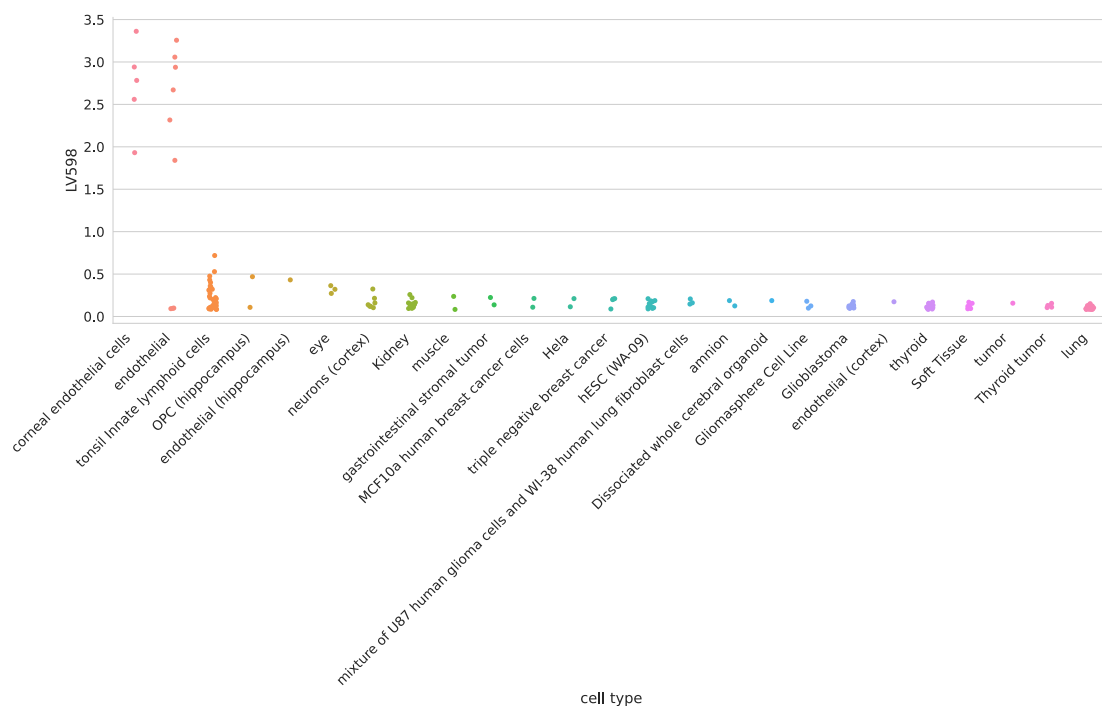| Trait description	Sample size	Cases	Partition/cluster number	p-value (adjusted)
Rheumatoid Arthritis	80,799	19,234	29 / 26	4.27e-57
Non-cancer illness code, self-reported: malabsorption/coeliac disease	361,141	1,587	29 / 8	4.83e-43
Coeliac disease	361,194	842	29 / 8	4.76e-41
Diagnoses - main ICD10: K90 Intestinal malabsorption	361,194	922	29 / 8	1.41e-39
Started insulin within one year diagnosis of diabetes	16,415	1,999	29 / 13	1.78e-37
Systemic Lupus Erythematosus	23,210	7,219	29 / 26	1.41e-34
Age diabetes diagnosed	16,166		29 / 13	3.93e-34
Never eat eggs, dairy, wheat, sugar: Wheat products	359,777	9,573	29 / 13	2.78e-31
Non-cancer illness code, self-reported: hyperthyroidism/thyrotoxicosis	361,141	2,730	29 / 13	6.08e-30
Treatment/medication code: insulin product	361,141	3,545	29 / 13	3.05e-25
Medication for cholesterol, blood pressure, diabetes, or take exogenous hormones: Insulin	193,148	1,476	29 / 13	4.63e-23
Medication for cholesterol, blood pressure or diabetes: Insulin	165,340	2,248	29 / 13	1.92e-20
Non-cancer illness code, self-reported: hypothyroidism/myxoedema	361,141	17,574	29 / 13	4.96e-20

Trait description	Sample size	Cases	Partition/cluster number	p-value (adjusted)
Treatment/medication code: levothyroxine sodium	361,141	14,689	29 / 13	4.01e-19
Non-cancer illness code, self-reported: psoriasis	361,141	4,192	29 / 13	9.28e-16

Table 16: Significant trait associations of LV844 in eMERGE.

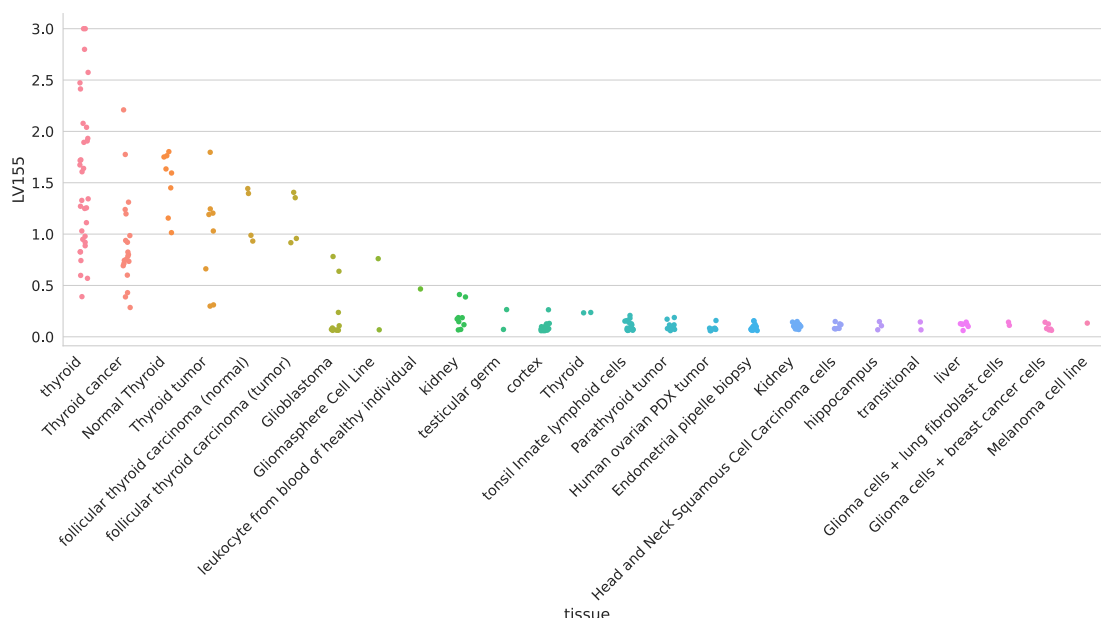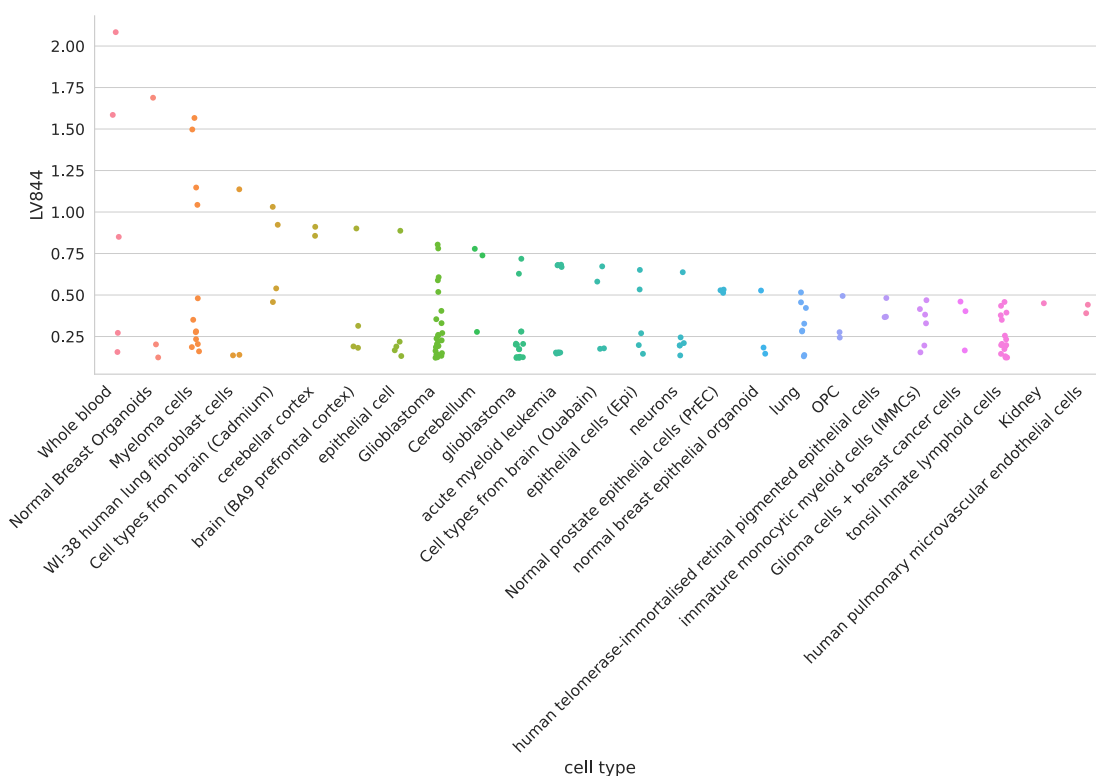| Phecode	Trait description	Sample size	Cases	p-value (adjusted)
714.1	Rheumatoid arthritis	49,453	2,541	8.22e-09
250.1	Type 1 diabetes	42,723	2,450	2.54e-08
714	Rheumatoid arthritis and other inflammatory polyarthropathies	50,215	3,303	5.06e-07
440	Atherosclerosis	47,471	4,993	3.15e-03
578.8	Hemorrhage of rectum and anus	47,545	1,991	3.15e-03
585.32	End stage renal disease	43,309	1,842	4.38e-03
440.2	Atherosclerosis of the extremities	45,524	3,046	5.00e-03
514.2	Solitary pulmonary nodule	50,389	2,270	6.16e-03
444	Arterial embolism and thrombosis	43,378	900	1.36e-02
558	Noninfectious gastroenteritis	40,177	3,191	2.94e-02
747.11	Cardiac shunt/ heart septal defect	58,364	1,037	3.60e-02
585	Renal failure	51,437	9,970	3.87e-02
443.9	Peripheral vascular disease, unspecified	46,926	4,448	4.43e-02

LV57

Figure 23: Cell types for LV57.

Table 17: Significant trait associations of LV57 in PhenomeXcan.

Trait description	Sample size	Cases	Partition/cluster number	p-value (adjusted)
Non-cancer illness code, self-reported: hypothyroidism/myxoedema	361,141	17,574	29 / 13	1.17e-24
Treatment/medication code: levothyroxine sodium	361,141	14,689	29 / 13	6.07e-23
Non-cancer illness code, self-reported: hyperthyroidism/thyrotoxicosis	361,141	2,730	29 / 13	1.16e-06
Started insulin within one year diagnosis of diabetes	16,415	1,999	29 / 13	8.17e-05
Treatment/medication code: insulin product	361,141	3,545	29 / 13	6.33e-04
Medication for cholesterol, blood pressure, diabetes, or take exogenous hormones: Insulin	193,148	1,476	29 / 13	1.13e-03
Medication for cholesterol, blood pressure or diabetes: Insulin	165,340	2,248	29 / 13	4.50e-03

Table 18: Significant trait associations of LV57 in eMERGE.

Phecode	Trait description	Sample size	Cases	p-value (adjusted)
244	Hypothyroidism	54,404	9,720	3.97e-09
244.4	Hypothyroidism NOS	53,968	9,284	3.97e-09
279	Disorders involving the immune mechanism	56,771	3,309	4.93e-03
514.2	Solitary pulmonary nodule	50,389	2,270	1.19e-02

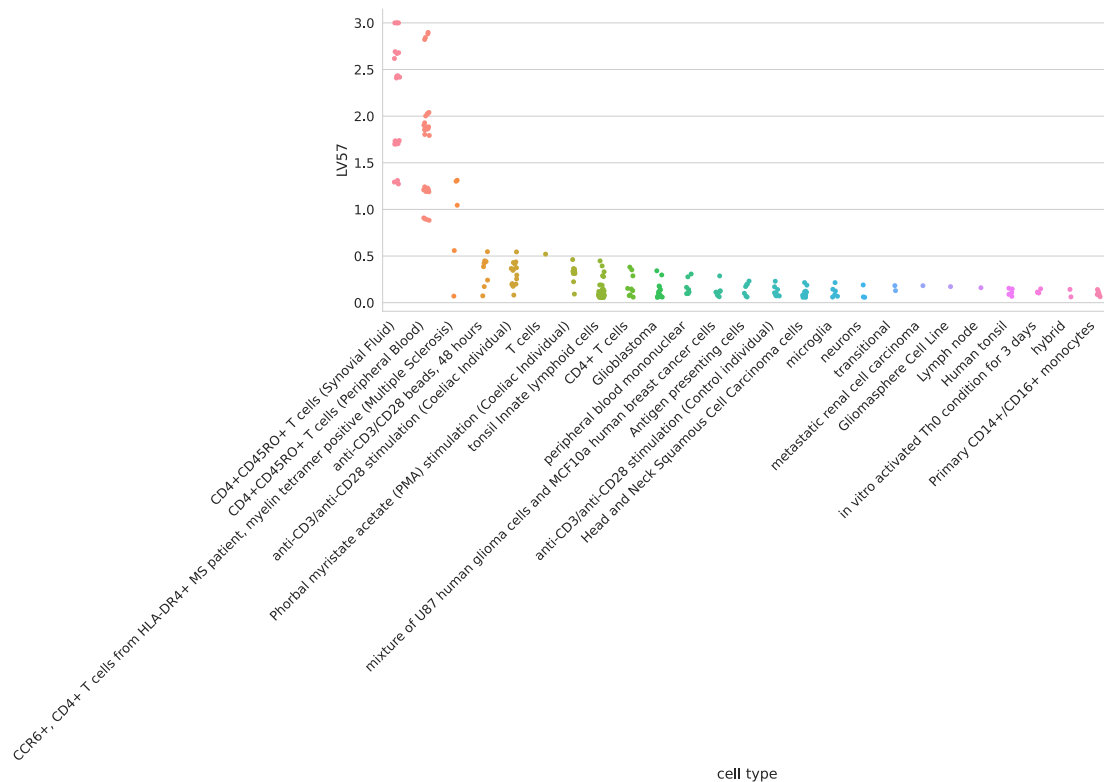| Phecode	Trait description	Sample size	Cases	p-value (adjusted)
714	Rheumatoid arthritis and other inflammatory polyarthropathies	50,215	3,303	1.68e-02
452.2	Deep vein thrombosis [DVT]	38,791	2,131	4.37e-02

LV54

Figure 24: Cell types for LV54.

Table 19: Significant trait associations of LV54 in PhenomeXcan.

Trait description	Sample size	Cases	Partition/cluster number	p-value (adjusted)
Diagnoses - main ICD10: K90 Intestinal malabsorption	361,194	922	29 / 8	5.09e-25
Coeliac disease	361,194	842	29 / 8	7.77e-25
Never eat eggs, dairy, wheat, sugar: Wheat products	359,777	9,573	29 / 13	6.33e-23
Systemic Lupus Erythematosus	23,210	7,219	29 / 26	1.32e-22
Started insulin within one year diagnosis of diabetes	16,415	1,999	29 / 13	3.84e-20
Non-cancer illness code, self-reported: hyperthyroidism/thyrotoxicosis	361,141	2,730	29 / 13	9.59e-19
Treatment/medication code: insulin product	361,141	3,545	29 / 13	5.07e-18
Age diabetes diagnosed	16,166		29 / 13	1.28e-17
Non-cancer illness code, self-reported: malabsorption/coeliac disease	361,141	1,587	29 / 8	1.36e-14
Medication for cholesterol, blood pressure or diabetes: Insulin	165,340	2,248	29 / 13	8.67e-14

Trait description	Sample size	Cases	Partition/cluster number	p-value (adjusted)
Non-cancer illness code, self-reported: psoriasis	361,141	4,192	29 / 13	2.61e-13
Rheumatoid Arthritis	80,799	19,234	29 / 26	3.11e-13
Medication for cholesterol, blood pressure, diabetes, or take exogenous hormones: Insulin	193,148	1,476	29 / 13	3.89e-12
Treatment/medication code: levothyroxine sodium	361,141	14,689	29 / 13	5.92e-10
Non-cancer illness code, self-reported: hypothyroidism/myxoedema	361,141	17,574	29 / 13	3.31e-08

Table 20: Significant trait associations of LV54 in eMERGE.

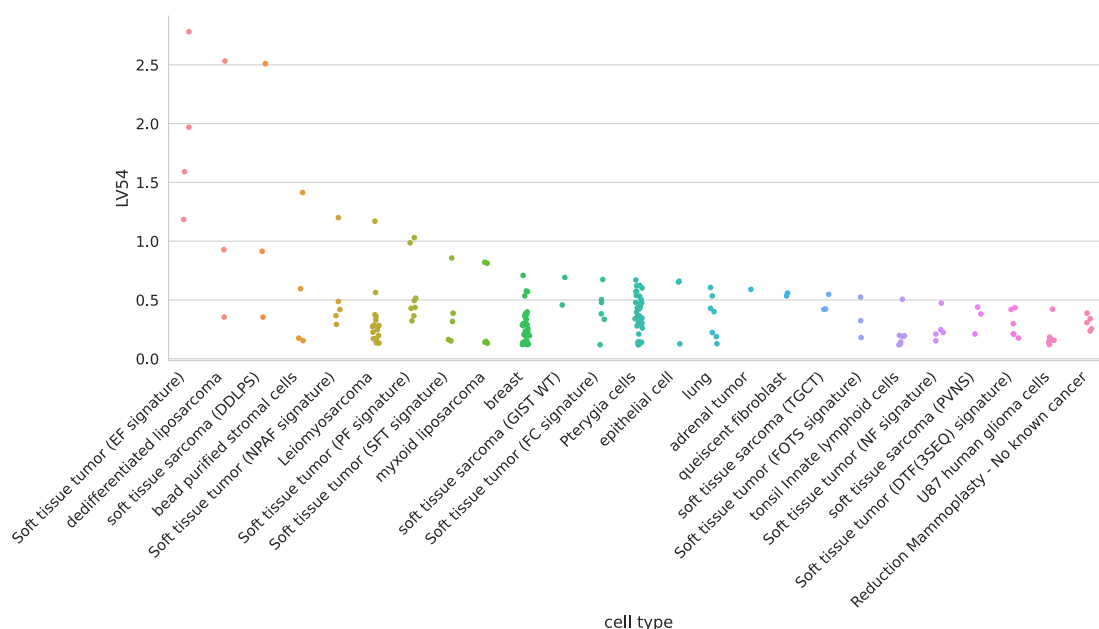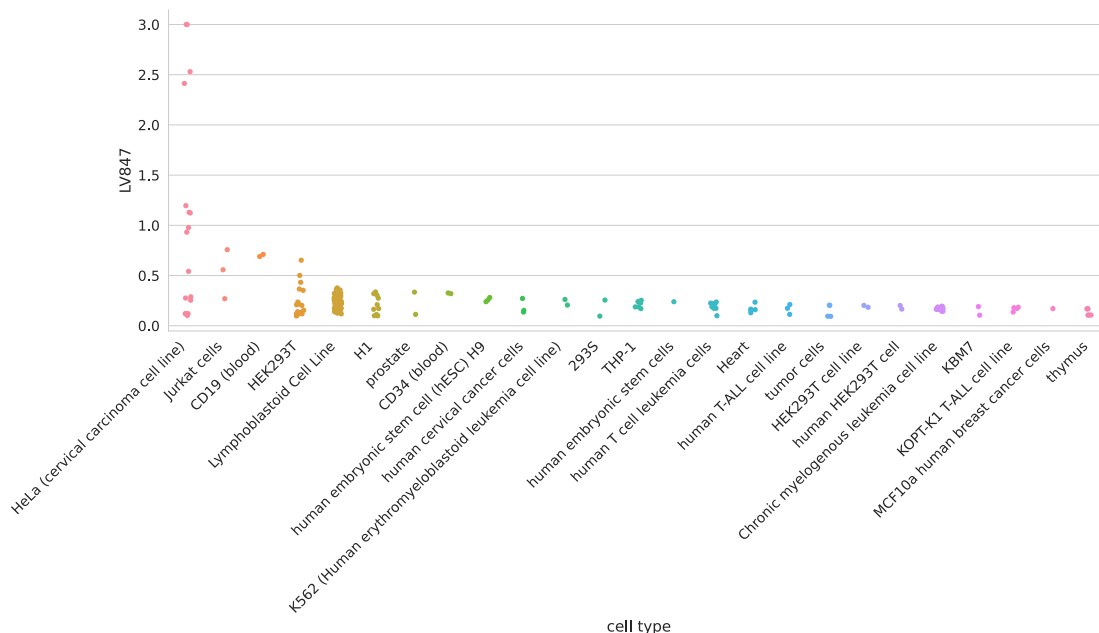| Phecode	Trait description	Sample size	Cases	p-value (adjusted)
250.1	Type 1 diabetes	42,723	2,450	2.04e-13
244	Hypothyroidism	54,404	9,720	5.10e-06
244.4	Hypothyroidism NOS	53,968	9,284	5.37e-06
695	Erythematous conditions	48,347	4,210	4.25e-05
714	Rheumatoid arthritis and other inflammatory polyarthropathies	50,215	3,303	3.06e-04
440	Atherosclerosis	47,471	4,993	8.88e-04
585	Renal failure	51,437	9,970	3.40e-03
585.32	End stage renal disease	43,309	1,842	3.64e-03
585.33	Chronic Kidney Disease, Stage III	46,279	4,812	3.64e-03
285.2	Anemia of chronic disease	39,673	2,606	7.62e-03
415.1	Acute pulmonary heart disease	49,887	1,857	8.67e-03
285.21	Anemia in chronic kidney disease	38,616	1,549	1.16e-02
743	Osteoporosis, osteopenia and pathological fracture	55,165	11,990	1.31e-02
415.11	Pulmonary embolism and infarction, acute	49,867	1,837	1.39e-02
577	Diseases of pancreas	60,538	1,795	1.42e-02
585.1	Acute renal failure	46,803	5,336	1.51e-02
195	Cancer, suspected or other	50,040	2,250	1.52e-02
440.2	Atherosclerosis of the extremities	45,524	3,046	1.89e-02
714.1	Rheumatoid arthritis	49,453	2,541	3.18e-02
458.9	Hypotension NOS	50,150	3,241	3.32e-02

LV847

Figure 25: **Cell types for LV847.**

Table 21: Significant trait associations of LV847 in PhenomeXcan.

Trait description	Sample size	Cases	Partition/cluster number	p-value (adjusted)
Medication for cholesterol, blood pressure, diabetes, or take exogenous hormones: Blood pressure medication	193,148	33,519	29 / 17	1.95e-18
Vascular/heart problems diagnosed by doctor: None of the above	360,420	253,565	29 / 17	4.07e-15
Vascular/heart problems diagnosed by doctor: High blood pressure	360,420	97,139	29 / 17	6.99e-14
Non-cancer illness code, self-reported: hypertension	361,141	93,560	29 / 17	1.48e-13
Treatment/medication code: bendroflumethiazide	361,141	20,196	29 / 17	1.41e-08
Medication for cholesterol, blood pressure or diabetes: Blood pressure medication	165,340	40,987	29 / 17	1.47e-07
Medication for cholesterol, blood pressure, diabetes, or take exogenous hormones: None of the above	193,148	133,338	29 / 17	1.55e-06
Diastolic blood pressure, automated reading	340,162		29 / 17	3.76e-06
Medication for cholesterol, blood pressure or diabetes: None of the above	165,340	110,372	29 / 17	6.36e-06

Table 22: Significant trait associations of LV847 in eMERGE.

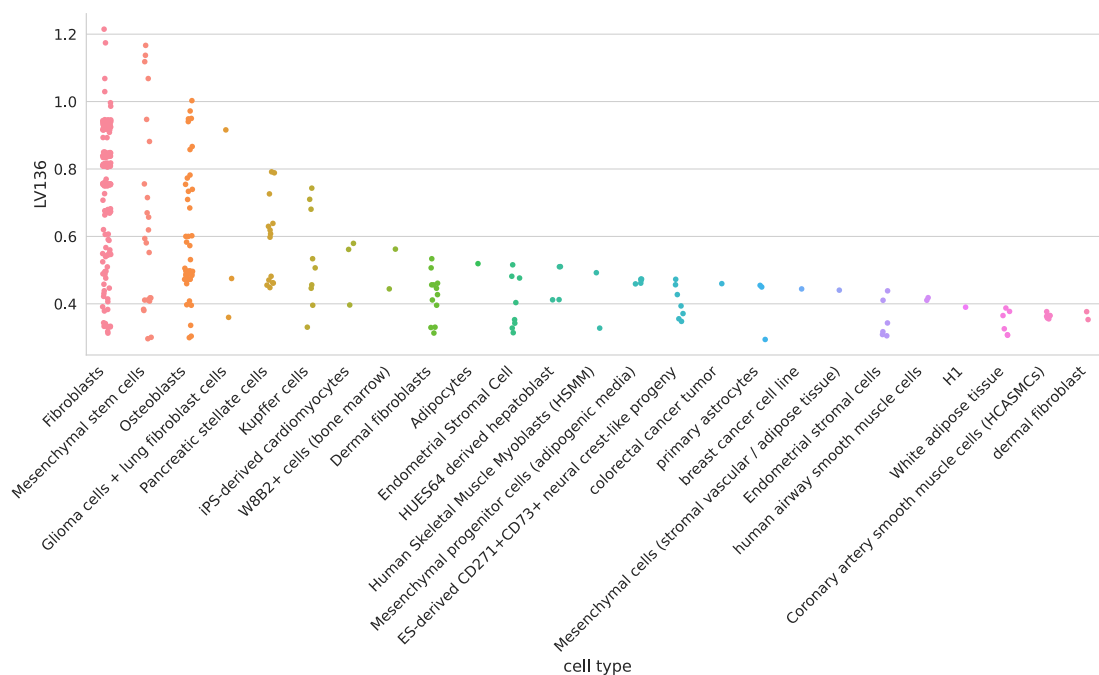| Phecode	Trait description	Sample size	Cases	p-value (adjusted)
585.32	End stage renal disease	43,309	1,842	1.88e-08
442.1	Aortic aneurysm	45,589	3,111	5.23e-06
411.3	Angina pectoris	43,503	4,382	2.14e-05
415.11	Pulmonary embolism and infarction, acute	49,867	1,837	5.13e-05
416	Cardiomegaly	53,289	5,259	6.50e-05
415.1	Acute pulmonary heart disease	49,887	1,857	7.28e-05
411	Ischemic Heart Disease	54,275	15,154	5.49e-04
401.2	Hypertensive heart and/or renal disease	30,405	6,253	1.28e-03
519	Other diseases of respiratory system, not elsewhere classified	56,909	2,056	1.28e-03
411.8	Other chronic ischemic heart disease, unspecified	44,123	5,002	1.42e-03
427.6	Premature beats	31,575	2,453	5.65e-03
687.1	Rash and other nonspecific skin eruption	47,039	4,964	9.88e-03
185	Cancer of prostate	52,630	2,815	1.03e-02
591	Urinary tract infection	49,727	10,016	1.34e-02
442.11	Abdominal aortic aneurysm	44,531	2,053	2.08e-02
427.21	Atrial fibrillation	37,743	8,621	2.26e-02
389.1	Sensorineural hearing loss	53,672	4,318	2.73e-02
427.2	Atrial fibrillation and flutter	37,934	8,812	4.50e-02

LV136

Figure 26: Cell types for LV136. Pulmonary microvascular endothelial cells were exposed to hypoxia for 24 hours or more [96];

Table 23: Significant trait associations of LV136 in PhenomeXcan.

Trait description	Sample size	Cases	Partition/cluster number	p-value (adjusted)
3mm strong meridian (right)	75,410		29 / 10	9.19e-11
6mm strong meridian (left)	65,551		29 / 10	2.06e-09
6mm strong meridian (right)	66,256		29 / 10	2.38e-09
3mm strong meridian (left)	75,398		29 / 10	1.34e-08
3mm weak meridian (right)	75,410		29 / 10	1.67e-08
Coronary Artery Disease	184,305	60,801	29 / 11	1.67e-08
6mm weak meridian (right)	66,256		29 / 10	3.21e-08
3mm weak meridian (left)	75,398		29 / 10	5.20e-08
6mm weak meridian (left)	65,551		29 / 10	1.21e-07
Coronary atherosclerosis	361,194	14,334	29 / 14	3.90e-06
Ischaemic heart disease, wide definition	361,194	20,857	29 / 14	7.22e-06
Vascular/heart problems diagnosed by doctor: Heart attack	360,420	8,288	29 / 14	2.93e-04
Myocardial infarction	361,194	7,018	29 / 14	6.33e-04
Myocardial infarction, strict	361,194	7,018	29 / 14	6.33e-04
Diagnoses - main ICD10: I21 Acute myocardial infarction	361,194	5,948	29 / 14	9.92e-04
Non-cancer illness code, self-reported: heart attack/myocardial infarction	361,141	8,239	29 / 14	1.40e-03
Major coronary heart disease event excluding revascularizations	361,194	10,157	29 / 14	1.85e-02
Major coronary heart disease event	361,194	10,157	29 / 14	1.85e-02
Fasting Insulin	38,238		29 / 11	3.85e-02

Table 24: Significant trait associations of LV136 in eMERGE.

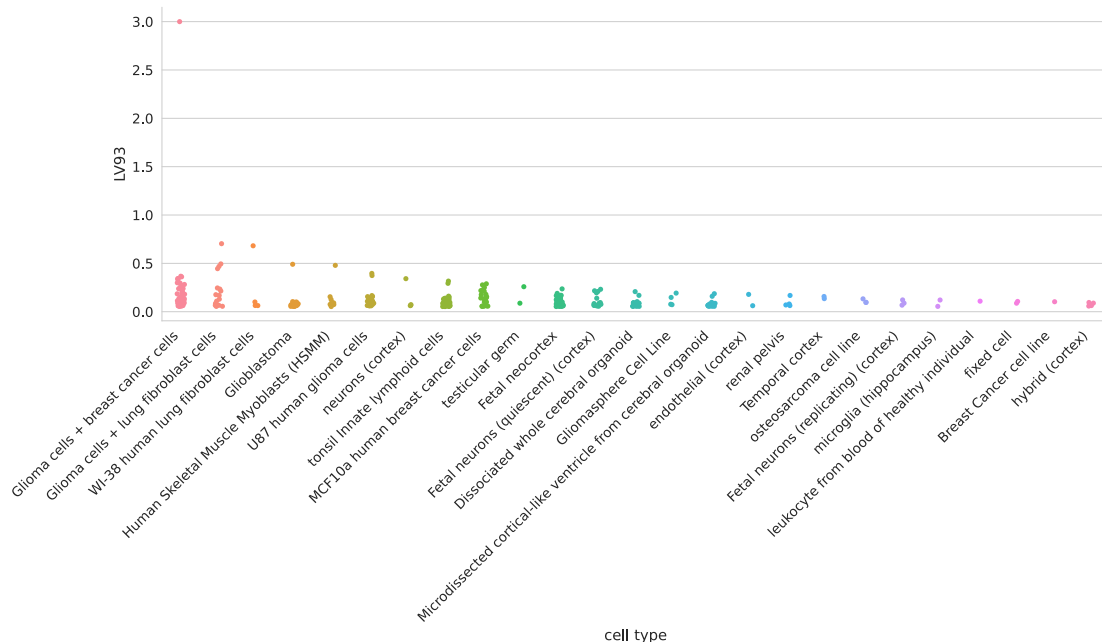| Phecode	Trait description	Sample size	Cases	p-value (adjusted)
747.1	Cardiac congenital anomalies	59,198	1,871	4.71e-02
411.4	Coronary atherosclerosis	52,836	13,715	4.80e-02

LV93

Figure 27: Cell types for LV93.

Table 25: Significant trait associations of LV93 in PhenomeXcan.

Trait description	Sample size	Cases	Partition/cluster number	p-value (adjusted)
CH2DB NMR	24,154		29 / 16	9.61e-24
Chronotype	128,266		29 / 16	1.17e-03
HDL Cholesterol NMR	19,270		29 / 16	2.99e-03

Table 26: Significant trait associations of LV93 in eMERGE.

Phecode	Trait description	Sample size	Cases	p-value (adjusted)
208	Benign neoplasm of colon	55,694	8,597	6.21e-03
440.2	Atherosclerosis of the extremities	45,524	3,046	1.31e-02
444	Arterial embolism and thrombosis	43,378	900	4.06e-02

LV206

Figure 28: Cell types for LV206.

Table 27: Significant trait associations of LV206 in PhenomeXcan.

Trait description	Sample size	Cases	Partition/cluster number	p-value (adjusted)
CH2DB NMR	24,154		29 / 16	7.67e-21
HDL Cholesterol NMR	19,270		29 / 16	6.46e-03

Table 28: Significant trait associations of LV206 in eMERGE.

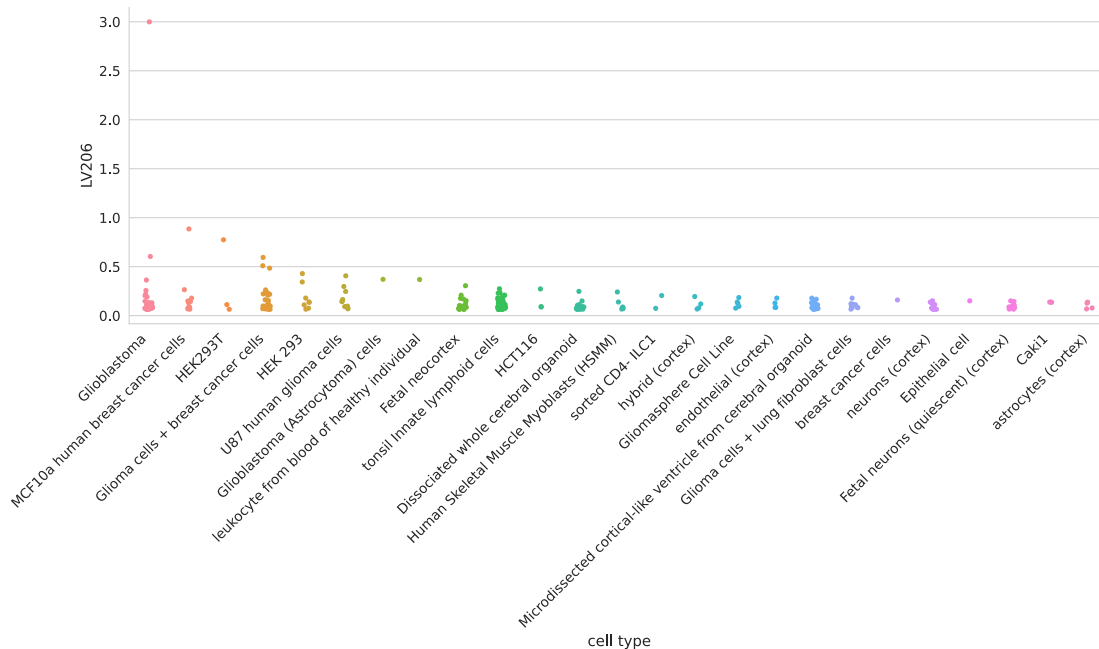| Phecode	Trait description	Sample size	Cases	p-value (adjusted)
458	Hypotension	51,341	4,432	1.41e-02
286.9	Abnormal coagulation profile	48,006	800	1.54e-02
458.9	Hypotension NOS	50,150	3,241	1.58e-02
428.2	Heart failure NOS	48,178	3,584	1.65e-02

LV260

Figure 29: Cell types for LV260.

Table 29: Significant trait associations of LV260 in PhenomeXcan.

Trait description	Sample size	Cases	Partition/cluster number	p-value (adjusted)
CH2DB NMR	24,154		29 / 16	5.96e-17
HDL Cholesterol NMR	19,270		29 / 16	2.37e-02

Table 30: Significant trait associations of LV260 in eMERGE.

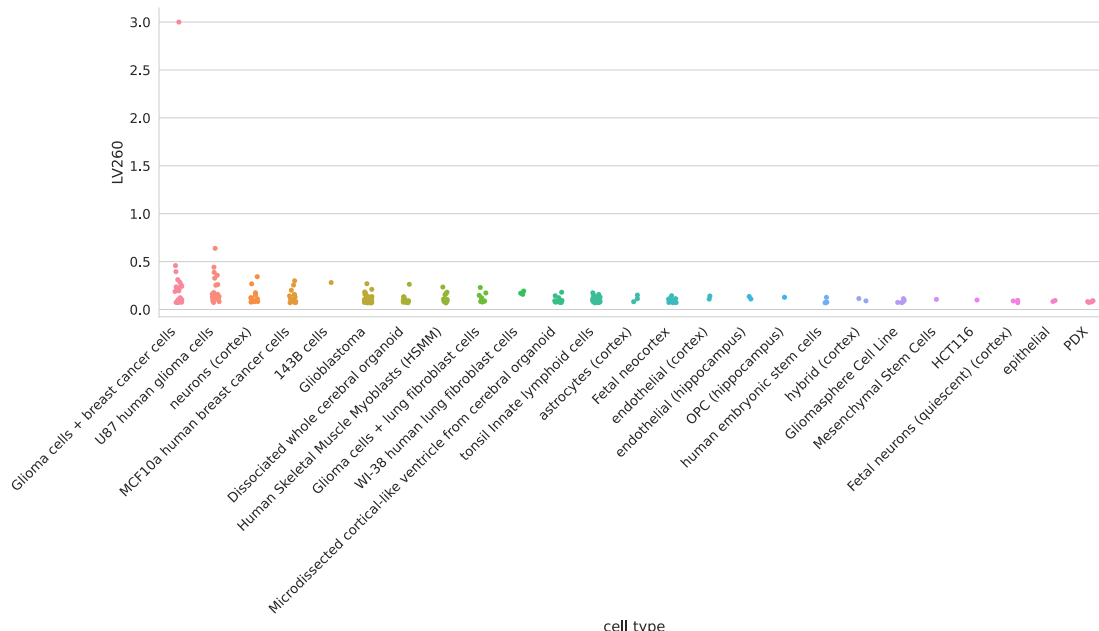| Phecode	Trait description	Sample size	Cases	p-value (adjusted)
427.6	Premature beats	31,575	2,453	2.85e-02
426.3	Bundle branch block	31,827	2,705	4.80e-02

LV21

Figure 30: Cell types for LV21.

Table 31: Significant trait associations of LV21 in PhenomeXcan.

Trait description	Sample size	Cases	Partition/cluster number	p-value (adjusted)
Alzheimers Disease	54,162	17,008	29 / 16	1.64e-19
LDL Cholesterol NMR	13,527		29 / 16	1.18e-04
Triglycerides NMR	21,559		29 / 16	2.19e-02

Table 32: Significant trait associations of LV21 in eMERGE.

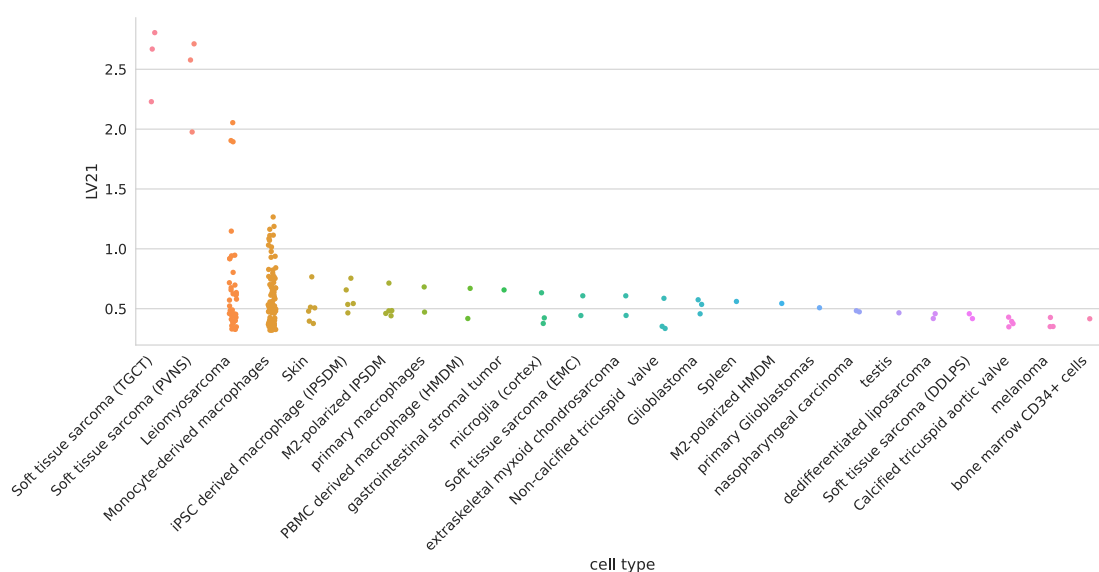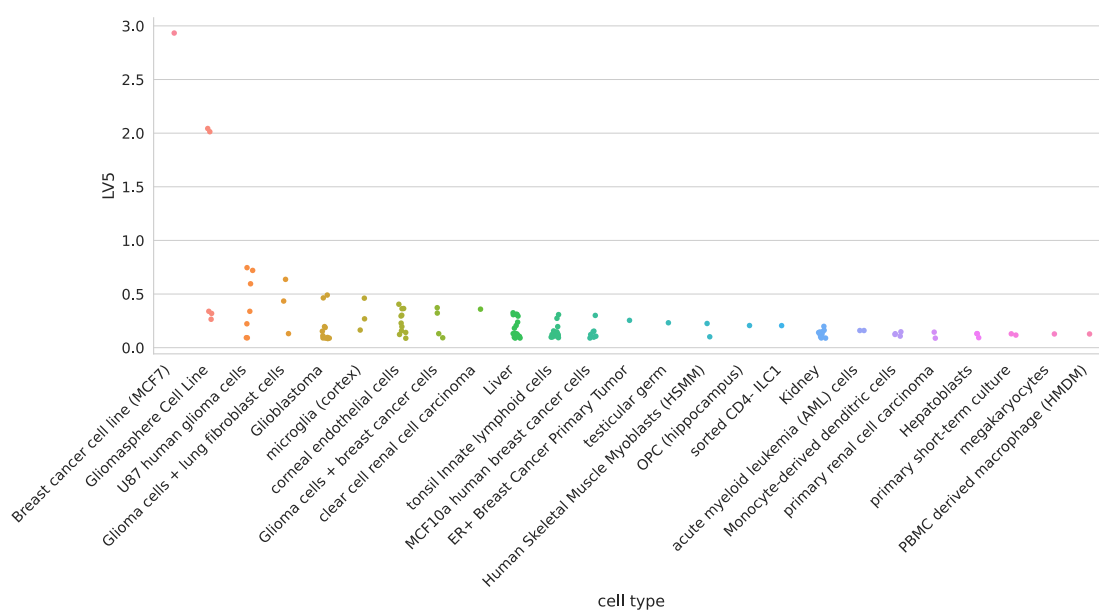| Phecode	Trait description	Sample size	Cases	p-value (adjusted)
573	Other disorders of liver	47,826	2,524	1.37e-02
577	Diseases of pancreas	60,538	1,795	2.15e-02

LV5

Figure 31: Cell types for LV5.

Table 33: Significant trait associations of LV5 in PhenomeXcan.

Trait description	Sample size	Cases	Partition/cluster number	p-value (adjusted)
LDL Cholesterol NMR	13,527		29 / 16	1.78e-04
Triglycerides NMR	21,559		29 / 16	5.00e-04
Alzheimers Disease	54,162	17,008	29 / 16	3.06e-03
Ever had prolonged feelings of sadness or depression	117,763	64,374	29 / 27	8.69e-03
Substances taken for depression: Medication prescribed to you (for at least two weeks)	117,763	28,351	29 / 27	1.03e-02
Recent feelings of depression	117,656		29 / 27	1.32e-02
Ever contemplated self-harm	117,610		29 / 27	1.89e-02
Recent lack of interest or pleasure in doing things	117,757		29 / 27	2.08e-02
Amount of alcohol drunk on a typical drinking day	108,256		29 / 27	3.50e-02

Trait description	Sample size	Cases	Partition/cluster number	p-value (adjusted)
Ever sought or received professional help for mental distress	117,677	46,020	29 / 27	3.92e-02
General happiness	117,442		29 / 27	4.74e-02

Table 34: Significant trait associations of LV5 in eMERGE.

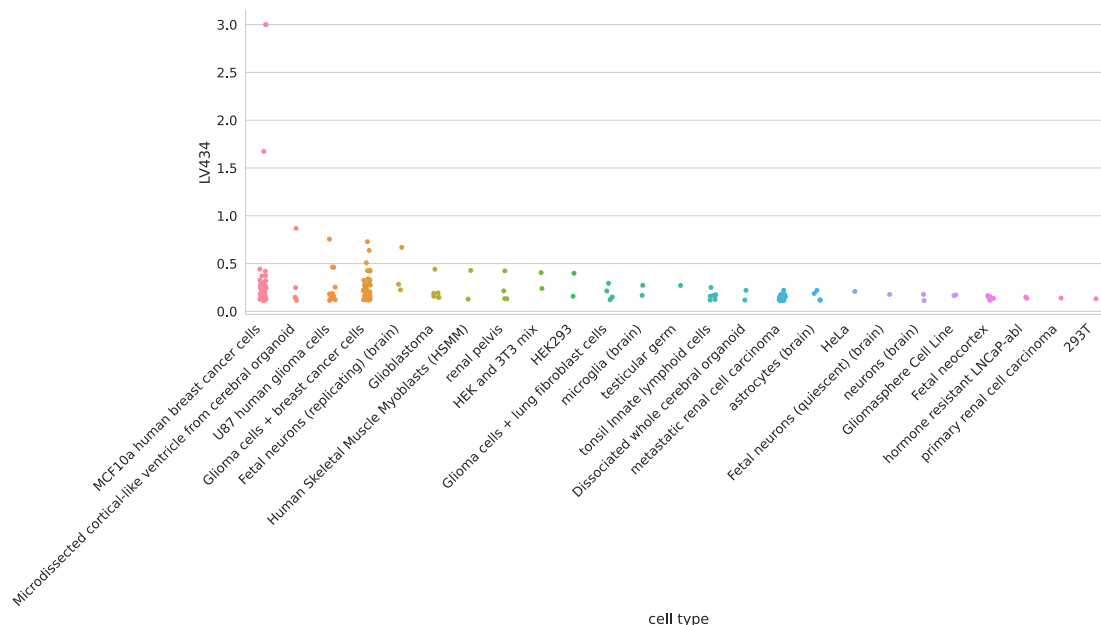| Phecode	Trait description	Sample size	Cases	p-value (adjusted)
241	Nontoxic nodular goiter	47,842	3,158	8.98e-03
241.1	Nontoxic uninodular goiter	47,125	2,441	2.57e-02
241.2	Nontoxic multinodular goiter	46,465	1,781	4.43e-02

LV434

Figure 32: Cell types for LV434. HEK293 is a cell line derived from human embryonic kidney cells; 3T3 is a cell line derived from mouse embryonic fibroblasts.

Table 35: Significant trait associations of LV434 in PhenomeXcan.

Trait description	Sample size	Cases	Partition/cluster number	p-value (adjusted)
Attention Deficit Hyperactivity Disorder	53,293	19,099	29 / 21	7.01e-03

Table 36: Significant trait associations of LV434 in eMERGE.

Phecode	Trait description	Sample size	Cases	p-value (adjusted)
722	Intervertebral disc disorders	47,659	7,458	6.65e-03
721	Spondylosis and allied disorders	47,517	7,316	7.62e-03
250.4	Abnormal glucose	45,220	4,947	1.02e-02
721.1	Spondylosis without myelopathy	47,315	7,114	1.22e-02
720	Spinal stenosis	44,807	4,606	1.74e-02

Phecode	Trait description	Sample size	Cases	p-value (adjusted)
288	Diseases of white blood cells	47,288	2,802	2.10e-02
796	Elevated prostate specific antigen [PSA]	51,990	2,175	3.09e-02
288.2	Elevated white blood cell count	46,595	2,109	3.54e-02
079	Viral infection	46,991	1,934	4.19e-02

Agreement of consensus clustering partitions with the ensemble by number of clusters
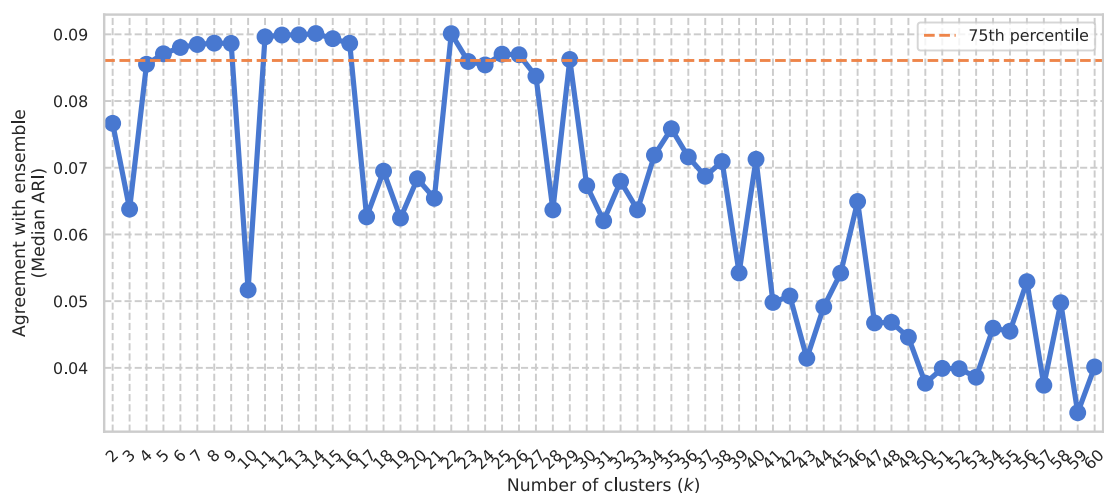

Figure 33: Final selected partitions for follow-up analysis. From all consensus clustering partitions generated with k from 2 to 60, we selected those with a median adjusted Rand index (ARI) with the ensemble members greater the 75th percentile.